CZECH UNIVERSITY OF LIFE SCIENCES

Faculty of Environmental Sciences

Department of landscape and urban planning

Assessing the impact of the tall buildings on urban heat island effect of adjacent built area, case of Prague 3, Czech Republic

Diploma Thesis

Thesis Supervisor: Doc. Peter Kumble Ph.D.

Author: Mahsa Hemmati

Prague

2024

CZECH UNIVERSITY OF LIFE SCIENCES

FACULTY OF ENVIRONMENTAL SCIENCES

DIPLOMA THESIS ASSIGNMENT

MAHSA HEMMATI, M.Sc

LANDSCAPE ENGINEERING
LANDSCAPE PLANNING

Thesis title:

Assessing the impact of the tall buildings on urban heat island effect of adjacent built area in Prague 3, Czech Republic

Preface:

One dimension of the urban environment that has received limited attention or has been overly simplified in numerous urban climate studies pertains to the release of heat and moisture connected with energy usage within urban areas. These emissions originate from various sources, including human activities, vehicles, both residential and commercial structures, industrial processes, and power plants. The release of sensible anthropogenic heat into the atmosphere can occur directly through outlets like tailpipes, chimneys, and air conditioning or heating systems, or it can happen indirectly through the conduction of heat through tall building structures, followed by convection and radiation into the urban surroundings (Sailor, 2011).

The urban heat island is a thermal irregularity that manifests across horizontal, vertical, and temporal dimensions and has been detected in nearly all urban areas, regardless of their size. In regions within the mid-latitudes where extensive research has been conducted, its attributes are observed to be connected to both inherent urban factors (such as city size, building density, and land-use distribution) and external factors (such as climate, prevailing weather conditions, and seasonal variations) (Oke, 1982).

Undoubtedly, the urban heat island is an extensively studied aspect of climate change, with comprehensive documentation available for diverse geographic regions worldwide. It's noteworthy that in numerous urban areas, the intensity of the heat island effect can surpass several degrees, and significant regional and temporal variations are evident. Alongside global climate change, the urban heat island plays a pivotal role in the substantial rise in urban temperatures. This phenomenon is particularly conspicuous in specific zones of cities characterized by high population density and low environmental quality, leading to a significant decrease in outdoor thermal comfort and unfavorable indoor thermal conditions. (Santamouris, 2015).

The Urban Heat Island (UHI) effect, arising from increased heat accumulation due to urban

development and human activities, significantly impacts urban climates and the associated ecological and environmental aspects. It results in elevated land surface temperatures, disrupting material and energy flow in urban ecosystems, thereby affecting their structure and functions, which, in turn, has repercussions on urban climates, hydrology, soil quality, atmospheric conditions, biodiversity, material cycles, energy consumption, and public health. Mitigation strategies encompass enhancing energy efficiency, optimizing urban design, employing green roofs, using reflective materials, and promoting green spaces. Research employing remote sensing and numerical simulations provides theoretical foundations for enhancing urban ecosystems and achieving sustainable urban development. The increasing urbanization has led to rising surface temperatures, altering resource and energy dynamics and affecting the structure and function of urban ecosystems and public health (Yang et al. 2016).

The UHI effect, receiving substantial attention from urban meteorologists, has been explored primarily from a non-ecosystem perspective, and its adverse effects include deteriorating living conditions, heightened energy consumption, elevated ground-level ozone concentrations, and increased mortality rates. Consequently, researchers and engineers are increasingly drawn to UHI mitigation strategies, with planting more vegetation being a widely reported measure. UHI challenges, rooted in urbanization and industrialization, are more acute in densely populated, economically active cities, directly impacting roughly three billion urban residents globally and intensifying with ongoing urbanization. Research findings underscore the UHI effect's association with factors like urban heat emissions, surface characteristics, vegetation cover, population density, and weather conditions, emphasizing the need for comprehensive mitigation efforts (Rizwan et al. 2008).

Objectives of thesis:

This thesis focuses on the critical aspect of UHI, highlighting the significance of heat re-radiation by urban high-rise structures in the capital city of the Czech Republic, Prague 3, and understanding urban heating, especially UHI. This thesis emphasizes the need for future research to concentrate on designing and planning parameters that can reduce the impact of the urban heat island, ultimately creating a better urban living environment in the research study area. The objective of this thesis is to perform a comprehensive analysis of the available data with regards to existing tall buildings in Prague 3, to devise possible sustainable solutions concerning mitigating UHI effects with green strategies.

Methodology:

The work is based on the combination of 3D visualization of the high-rise buildings located in Prague 3, Czech Republic, utilizing QGIS and Google Earth Pro. The mentioned procedure involves visualization of Intended tall buildings and analyzing them against heating effect with the data from geoportal Praha.

This thesis will examine the impact of city towers, skyscrapers, or even slightly tall buildings in Prague 3, on their surrounding urban spaces, in terms of urban heat island. It is highly possible that the UHI is not much raised in pavements and streets around such buildings owing to the shadows provided by the same building. However, the building itself will have a considerable increase in temperature due to many reasons such as more energy consumption,

dense urban environment, larger surface area exposed to sun, etc. Following the in-depth data analysis, feasible mitigation plans through optimization of the construction processes will be presented.

The proposed extent of the thesis:

45 Pages

Keywords:

Urban planning, Urban heat island effects, Urban environment, Geospatial analysis, Spatial planning

Recommended information sources

- Memon, Rizwan & Leung, Dennis & Chunho, Liu. (2008). A review on the generation, determination, and mitigation of Urban Heat Island. Journal of Environmental Sciences (China). 20. 120-128
- Oke, T. R. (1982). The energetic basis of the urban heat island. Quarterly journal of the royal meteorological society, 108(455), 1-24.
- Sailor, D. J. (2011). A review of methods for estimating anthropogenic heat and moisture emissions in the urban environment. International journal of climatology, 31(2), 189-199.
- Santamouris, M. (2013). Using cool pavements as a mitigation strategy to fight urban heat island—A review of the actual developments. Renewable and Sustainable Energy Reviews, 26, 224-240.
- Yang, L., Qian, F., Song, D. X., & Zheng, K. J. (2016). Research on urban heat-island effect. Procedia engineering, 169, 11-18.

Expected date of thesis defence
2023/24 SS – FES

Supervising department
Department of Landscape and Urban Planning

The Diploma Thesis Supervisor
Doc. Peter Kumble, Ph.D.

Consultant of thesis
Ph.D. candidate Masoud Barikani

DIPLOMA THESIS AUTHOR'S DECLARATION

ACKNOWLEDGEMENTS

ABSTRACT

Urbanization and industrialization, while improving our well-being, present challenges like global warming and air pollution. These issues are particularly severe in cities with intense human activity, where natural environments are disrupted.

A major consequence is the Urban Heat Island (UHI) effect, causing higher temperatures in cities compared to surroundings. This is caused by heat released from vehicles, buildings, and power plants, along with reduced heat dissipation due to less vegetation and dense urban structures.

The UHI effect worsens air quality, increases energy consumption, and even raises mortality rates. Scientists are actively researching mitigation strategies, and planting more vegetation is seen as a promising solution.

This thesis reviews existing literature on UHI, focusing on the heat re-radiated by urban structures. The research emphasizes the need for further investigation into design and planning solutions to minimize UHI impacts and create healthier urban environments.

ABSTRAKT

Urbanizace a industrializace sice zlepšují naši životní úroveň, ale přinášejí také výzvy, jako je globální oteplování a znečištění ovzduší. Tyto problémy jsou obzvláště závažné ve městech s intenzivní lidskou činností, kde dochází k narušení přírodního prostředí.

Jedním z hlavních důsledků je jev městského tepelného ostrova (UHI), který způsobuje vyšší teploty ve městech oproti okolí. To je způsobeno teplem uvolňovaným z vozidel, budov a elektráren, spolu se sníženým odvodem tepla kvůli menší vegetaci a husté městské zástavbě.

Efekt UHI zhoršuje kvalitu ovzduší, zvyšuje spotřebu energie a dokonce zvyšuje úmrtnost. Vědci aktivně zkoumají zmírňovací strategie a výsadba většího množství vegetace je považována za slibné řešení.

Tato práce zkoumá stávající literaturu o UHI s důrazem na teplo znovu vyzařované městskými strukturami. Výzkum zdůrazňuje potřebu dalšího zkoumání návrhů a plánovacích řešení s cílem minimalizovat dopady UHI a vytvořit zdravější městské prostředí.

CONTENTS

Contents

1. Introduction

Urbanization and industrialization contribute significantly to our well-being and comfort, yet they also give rise to a multitude of challenges for humanity. These challenges include global warming, industrial waste, and air pollution. While these issues have global implications, their impact is particularly pronounced in urban areas characterized by intense industrial activities and widespread use of synthetic construction materials. Consequently, the natural environment and ecological balance in these regions are severely disrupted.

The consequences of urbanization problems are exacerbated by the escalating urban population, estimated at 48% or three billion, and projected to reach five billion by 2030 (World Urbanization Prospectus, 2004). In large cities, two distinct phenomena are observed when compared to their surroundings: Urban Heat Island (UHI), characterized by higher temperatures, and occasionally, Urban Cool Island (UCI) or Urban Cool Valley (UCV) featuring lower temperatures. The heightened urban heat is primarily attributed to anthropogenic heat released from sources like vehicles, power plants, and air conditioners. Additionally, it results from heat stored and re-radiated by the massive and intricate urban structures.

Urban areas exhibit higher heat retention due to the substantial construction material and reduced sky view factor, limiting heat dissipation. Furthermore, the diminished vegetation in urban settings and high roughness structure hinder convective heat removal. Mitigating strategies involve reducing anthropogenic heat release and implementing design changes, such as employing high albedo, cooler roofs, suitable building materials, and efficient building designs.

The adverse effects of UHI encompass the degradation of the living environment, heightened energy consumption (Konopacki and Akbari, 2002), elevated ground-level ozone (Rosenfeld et al., 1998), and even increased mortality rates (Changnon et al., 1996). The UHI field has gained significant interest from scientists and engineers due to its detrimental environmental and economic impacts, as well as the potential benefits associated with mitigating high heat intensity. Extensive literature review indicates that planting more vegetation is widely recognized as a promising mitigation measure (Tong et al., 2005; Ca et al., 1998; Ashie et al., 1999; Yu and Hien, 2006), although other proposed measures cover various aspects.

For instance, Konopacki and Akbari (2002) demonstrated that mitigating UHI effects in Houston could lead to savings of USD 82 million, a reduction of 730 MW peak power, and an annual decrease of 170,000 tons of carbon emissions. Rosenfeld et al. (1998) predicted that by reducing UHI, there could be an annual reduction of 25 GW of electrical power, translating to potential savings of USD 5 billion for the US by 2015. The substantial research in this field underscores its importance, although the intricate conditions of typical cities make simple methods for understanding, quantifying, and mitigating UHI rare. This paper seeks to provide a comprehensive review of available literature on UHI generation, determination, and mitigation, summarizing key findings, presenting the problem systematically, and discussing potential future research areas.

The Urban Heat Island (UHI) stands out as a significant challenge in the 21st century, emerging from the rapid urbanization and industrialization of human societies. This issue arises due to the substantial heat produced by urban structures, absorbing and releasing solar radiation, along with human-made heat sources. These dual contributors elevate temperatures in urban areas compared to their surroundings, known as Urban Heat Island Intensity (UHII). The predicament intensifies in densely populated cities with extensive economic activities.

Approximately three billion people residing in global urban areas directly face this problem, and this number is anticipated to rise significantly (Rizwan et al., 2008). Recognizing the severity of the issue, extensive research has been dedicated to exploring various aspects, including recent research approaches, concepts, methodologies, investigation tools, and measures to mitigate UHI effects. This study aims to review and summarize research, with a particular focus on a crucial aspect of UHI – the heat re-radiated by urban structures on the adjacent built environment.

The findings highlight that the heat re-radiation from urban structures plays a pivotal role and warrants detailed investigation to better understand urban heating, especially UHI. Additionally, it is emphasized that future research efforts should prioritize examining design and planning parameters aimed at minimizing the impacts of the urban heat island, ultimately contributing to a healthier living environment.

2. Objectives

The objective of this research is to assess the impact of the tall buildings on urban heat island effect of adjacent built area, case of Prague, Czech Republic, with a focus on the challenges and opportunities for the urban spaces and built environment.

The objective is to delve into the intricacies of how these towering structures contribute to the phenomenon of heightened temperatures in urban spaces and the built environment.

By undertaking a detailed analysis, the research seeks to uncover both the challenges and opportunities associated with the impact of tall buildings on the UHI effect. Understanding these dynamics is crucial for informing urban planning and design decisions that can effectively address and mitigate the heat-related challenges faced by cities, particularly in locations with a similar urban landscape as Prague.

In essence, this study aims to provide an examination of the relationship between tall buildings and the Urban Heat Island effect, offering valuable insights that can guide sustainable and resilient urban development practices in the face of ongoing urbanization and climate challenges.

In this framework, The research will be based on the following framework:

1. Literature Review: Conduct a thorough examination of existing academic works concerning the influence of tall buildings on the Urban Heat Island effect in adjacent built areas. This will encompass scientific and technical aspects, aiming to consolidate current knowledge in the field.

2. Data Collection: Gather observational data on heat patterns within the built environment surrounding tall buildings in Prague. Utilize sources such as satellite imagery, weather station data, and other pertinent information to compile a

comprehensive dataset for analysis.

3. Modeling: Develop and employ numerical models to simulate how heat patterns evolve in the built environment under varying climate scenarios. Validate these models by comparing their outputs with the observational data collected during the study.

4. Analysis: Scrutinize the results obtained from both modeling and data collection to pinpoint the key factors influencing heat distribution and the built environment. Evaluate the effectiveness of green systems and other adaptation measures in mitigating the Urban Heat Island effect.

5. Impacts Assessment: Assess the social and economic repercussions of climate change on urban spaces, with a specific focus on its effects on local communities, operators, and other stakeholders. Examine how the Urban Heat Island effect influences various facets of urban life.

6. Recommendations: Formulate practical recommendations for real estate developers and other stakeholders to enhance the resilience and sustainability of urban areas amidst ongoing urbanization. Provide actionable insights based on the study's findings.

7. Conclusions: Summarize the essential findings and recommendations derived from the research. Identify potential areas for future investigation, contributing to the continuous development of knowledge in the field of tall buildings and their impact on urban heat islands.

3. Literature review

This section serves as a condensed overview of research papers and writings authored by significant groups in the field of urban planning. Its aim is to introduce fundamental concepts and principles frequently addressed in related literature.

3.1 Theoretical foundation

The ecological environment plays a crucial role in human survival and development, significantly influencing the trajectory of civilizations (Hansen et al., 2018). However, the process of modern urbanization has disrupted natural surface patterns like water permeability or, paved surfaces resulting in elevated temperatures within urban areas compared to rural regions—a phenomenon commonly referred as the Urban Heat Island (UHI) effect (Li et al., 2022).

In recent times, a surge in extreme weather events has posed threats to human health, societal stability, and has led to substantial economic losses (Easterling et al., 2000; Luber & McGeehin, 2008; Peterson et al., 2013). As a consequence, UHI has emerged as a prominent topic in governmental, public, and academic discussions. Its far-reaching effects on health, society, economics, and ecosystems during extreme weather conditions are well-documented, particularly concerning the temperature response to various human activities (White et al., 2006; Schlenker & Roberts, 2009).

The urban thermal environment and the built-up landscape are intricately linked (Xu et al., 2019). The configuration of the urban built-up environment significantly

impacts residential thermal comfort and urban energy consumption (Elraouf et al., 2022; Xue et al., 2022). A well-designed built-up environment is paramount for urban development, shaping the city's structure and circulation. Notably, main urban areas often exhibit a denser built-up landscape compared to non-main urban areas, establishing a robust connection between UHI intensity and the built-up environment in these regions.

In light of these observations, future urban planning efforts should pragmatically incorporate the transformation and optimization of the built-up environment. This strategic approach is vital for effectively mitigating the adverse impacts of the Urban Heat Island phenomenon (UHI) on various facets of urban life.

3.1.1 UHI and connected phenomeno

Urban Heat Island (UHI) refers to the phenomenon where urban areas experience higher temperatures compared to their suburban and rural surroundings. This arises from an imbalance in the urban environment, marked by increased heat absorption, such as heightened solar radiation and anthropogenic heat, coupled with reduced thermal losses (James, 2001). UHI stands as a well-documented consequence of climate change, evident across various geographical regions (Santamouris, 2007; Akbari et al., 1992). In many cities, the intensity of the UHI can surpass several degrees of Celsius, displaying notable regional and temporal variations (Giannopoulou et al., 2011).

The implications of UHI extend beyond local weather patterns and are significant contributors to the observed escalation in urban temperatures (Founda, 2011; Asimakopoulos et al., 2012; Livada et al., 2007). Particularly in densely populated areas with lower environmental quality, UHI adversely impacts ambient thermal comfort and indoor conditions (Mihalakakou 2002; Sakkaet al., 2012). Disturbingly, the Center for Disease Control and Prevention in the United States estimated approximately 7,421 deaths between 1979 and 1998 resulting from excessive heat exposure as a consequence of UHI and growth of temperature (Cleveland, 2007).

UHI also significantly influences building energy consumption, doubling the cooling energy needs of structures due to the heightened urban temperatures (Hassid et al., 2012). Simultaneously, increased urban temperatures contribute to elevated emissions of urban pollutants, especially tropospheric ozone, with a consequential growth in the ecological footprint of heat island-affected cities (Stathopoulou et al., 2008).

Addressing the effects of UHI stands as a paramount priority for the scientific community, with several successful proposed mitigation techniques and technologies (Santamouris et al., 2007). These strategies involve the application of cool materials, characterized by high reflectivity in the solar spectrum and high thermal emissivity (Kolokotsa, 2012). Additionally, smart materials with advanced optical and thermal properties (Karlessi et al., 2009), urban green spaces with suitable landscaping and design, and the use of heat sinks utilizing the ground, ambient air, and water contribute to effective UHI control. Proper shading and solar control of urban

surfaces, along with the use of low-temperature roofs, whether with cool materials or through green or planted roofs, further contribute to UHI mitigation efforts.

A critical aspect of the UHI effect involves the impact of pavements on urban heat development. Recent studies underscore the determinant role of paved surfaces in the overall urban thermal balance (Sailor et al., 1995). Paved surfaces, constituting a substantial portion of the urban fabric, significantly contribute to the development of the heat island. Pavements in Europe and the USA, predominantly composed of concrete and asphalt, exhibit high surface temperatures during the summer (Rose et al., 2003). These surfaces cover a considerable percentage of urban areas, emphasizing their importance in understanding and addressing UHI.

Decreasing the surface temperature of pavements emerges as a viable strategy to improve thermal conditions in heat-affected cities. This can be achieved through the replacement of conventional paving surfaces with those exhibiting lower temperatures, reconstruction and rehabilitation of existing pavements to enhance thermal performance, and shading of paved surfaces to reduce solar radiation absorption. Cool pavements, categorized as reflective pavements with high solar albedo and thermal emissivity or water retention pavements using water evaporation to lower surface and ambient temperatures, have been developed and are available for use in urban environments. These technologies show promise, with many commercial products available and successful large-scale applications reported in Japan and elsewhere (Gaitani et al., 2011).

3.2 Pavements and urban climate

Pavements play a significant role in shaping the urban climate, and their thermal equilibrium is influenced by various factors such as absorbed solar radiation, emitted infrared radiation, convective heat transfer to the atmospheric air, heat stored within the material, and heat conducted to the ground. Anthropogenic heat, particularly from road traffic, can further impact the thermal balance of pavements. Specific studies, as reported in, indicate that infrared radiation from pavements in Tokyo contributes substantially to heating the atmosphere, accounting for about half the energy consumption rate of commercial areas in the city. Consequently, pavements emerge as major contributors to the development of the Urban Heat Island effect (Torbjörn and Bjorn, 2001).

Analyzing the thermal balance of pavements and their impact on the urban climate involves both experimental and computational simulation techniques. Experimental evaluation of pavement surface thermal regimes can be conducted using mesoscale remote sensing techniques or microscale measurement methods, including infrared thermography and conventional temperature monitoring. Mesoscale satellite-based techniques have been widely utilized to assess surface temperatures in urban areas. While satellite-based methods offer valuable insights into the spatial distribution of urban surface temperatures and early assessments of pavement material impacts on Urban Heat Islands, they are subject to constraints such as time limitations due to satellite orbits, image resolution, and interpretation challenges (Golden and Kaloush, 2006).

Microscale measurement techniques, employing infrared thermography or conventional temperature measurements with thermocouples, provide detailed information about the thermal conditions of studied areas, allowing for a deep understanding of corresponding thermal processes. Accurate measurement using infrared thermography requires precise knowledge or estimation of material emissivity, and methods for estimating material emissivity are presented in (Buettner and Kern, 1965). The use of thermocouples for surface temperature measurement is a well-established and accurate technique, contingent on achieving a strong contact between the surface and the sensors. Comparative measurements of surface temperatures for various pavement materials using both infrared thermography and conventional temperature sensors have shown temperature differences ranging from 0.2 to 5.6°K (Golden and Kaloush, 2006). In these comparisons, infrared thermography typically indicates higher temperatures than those recorded by thermocouple sensors. While microscale techniques offer a high degree of accuracy and instantaneous results on the diurnal temperature variations, they may fall short in providing a comprehensive visualization of temperature distribution across a large area.

Computational simulation techniques have been proposed and developed to predict and analyze the thermal performance of pavements. These models, utilizing analytical or numerical techniques (Qin and Hiller, 2011), vary in complexity. Many claim a good agreement with experimental data, offering a valuable tool for investigating specific thermal phenomena that may not be directly measurable.

3.2.1 The role of the albedo

The degree to which a material absorbs or reflects solar radiation depends on its spectral and broadband absorptivity or reflectivity. Information on the specific reflectivity of materials used in pavements and roads can be found in (Santamouris 2001). Generally, the reflectivity value is influenced by the material's color and surface roughness. Light-colored materials exhibit lower absorptivity in the visual spectrum of solar radiation, while the specific absorptivity in the infrared part of the radiation is relatively independent of perceived color. The roughness of the surface also affects the absorptivity of solar radiation, as observed in (Doulos, 2004), where tiles with smooth and flat surfaces were cooler than those with rough and anaglyph surfaces.

Numerous studies have sought to correlate the impact of pavement material color on surface temperature and released sensible heat. In (Doulos, 2004), several types of commercial pavements were comparatively tested during the summer. The maximum surface temperature difference between black granites and white marbles reached values close to 19.1°K, with significant temperature differences observed between pavements of different colors. In (Synnefa et al., 2011), the surface temperature of different-colored thin-layer asphaltic materials exposed to solar radiation was measured. Off-white asphalt in Los Angeles, with a visible albedo close to 0.45, was found to have almost 12°K lower maximum surface temperature than black asphalt with an albedo close to 0.03. Similarly, yellow, beige, green, and

red asphalt materials with albedos in the visual spectra presented lower maximum surface temperatures than black asphalt, indicating that the specific reflectivity value of the materials in the near infrared part of the spectrum affected surface temperature almost equally (GMCCX, 2017).

Measurements conducted in street canyons (Niachou et al., 2008) during summer showed that the surface temperature of black asphalt reached temperatures close to 65.1°C, gray stone was 48.1°C, and the surface temperature of shaded and non-shaded gray color cement pavements was around 30°C and 60°C, respectively. Another study (Berg and Quinn, 1978) involving painted streets with an albedo of 0.55 against unpainted streets with an albedo close to 0.15 showed that high albedo streets presented almost 11K lower ambient temperature. Sensible transport and emissions measurements from asphalt pavements and bare soil are reported in [79]. Asphalt pavements contributed an additional 200W/m² in sensible transport and emitted plus 150W/m² in infrared radiation compared to bare soil. Other measurements reported in showed that white elastomeric coatings with an albedo of 0.72 were 45K cooler than black coatings with an albedo of 0.08.

A comparative assessment of different pavement materials used in the urban environment of Athens, Greece, using satellite remote sensing techniques during the hot summer period is reported in (Sthathopoulou, 2009). The surface temperature of asphalt measured between 77.6°C and 81.8°C, concrete between 56.2°C and 78.6°C, marble between 48.6°C and 67.3°C, and stone between 47.5°C and 75.1°C. Comparative measurements of various pavement materials during the summer period are reported in (Golden and Kaloush, 2006). In particular, conventional graded hot mix asphalt, asphalt rubber chip seal, gap-graded asphalt rubber mixture, plain concrete pavement sections, and plain concrete sections modified with the use of crumb rubber were measured. The gap-graded asphalt rubber concrete presented the highest surface temperature (67.8°C) and the lowest albedo (0.12). The pavement made of concrete section had the highest albedo (0.48) and a surface temperature close to 51.8°C.

It is noteworthy that the surface temperature of thick asphalt rubber was close to 66.7°C for an albedo of 0.13 and was reduced to 51.1°C when the albedo increased to 0.26 by adding some white paint. A sensitivity analysis regarding the impact of the albedo on the maximum and minimum surface temperature of various pavement materials is reported in. It was found that materials with albedos close to 0.1 and 0.5 had surface temperatures close to 71°C and 53°C, respectively, while the corresponding minimum surface temperatures were 67°C and 60°C. Research reported in (Pomerantz et al., 1997) shows that pavements presenting albedos of 0.05, 0.15, and 0.35 had a surface temperature equal to 50.5°C, 46.1°C, and 32.2°C, respectively.

Significant research efforts to increase the reflectivity of paving materials are underway and reported. Technological developments focus on two different directions:

(a) increasing the albedo of light-colored or white pavements by enhancing their spectral reflectance in the visible part of the solar radiation and (b) increasing the

spectral reflectivity of colored materials in the near-infrared part of the spectrum. A review of the existing recent developments is given in the following sections.

3.2.2 The role of the emissivity

Materials emit longwave radiation based on their temperature and emissivity. High emissivity values indicate good emitters of longwave radiation, allowing them to readily release absorbed energy. Simulations of emitted thermal radiation from pavements in California demonstrated that the net infrared radiation balance varied between 60 and 120 W/m² depending on the surface temperature (Qin and Hiller, 2001). Similar measurements reported in (Asaeda et al., 1996) indicated that the maximum upward infrared radiation over asphalt and normal color concrete was around 550 W/m², while the net infrared radiation balance varied between 0.0 and 80 W/m².

Various studies have explored the impact of emissivity on the thermal performance of materials in the urban environment. Surface temperature measurements of highly reflective paving materials (Synnefa et al., 2006) concluded that emissivity is the most crucial factor influencing material surface temperature during the night. A strong correlation was found between the average nocturnal surface temperature and the corresponding material emissivity. Materials with an emissivity of 0.93 exhibited a nighttime surface temperature depression of 5°K compared to other materials with emissivity close to 0.35. A sensitivity analysis in (Gavin et al., 2007) regarding the role of emissivity on the maximum and minimum surface temperature of various pavement materials showed that increasing the emissivity value from 0.7 to 1.0 led to decreases of 5.0°K and 8.5°K, respectively.

In (Shi and Zhang, 2011), the combined impact of surface reflectivity and emissivity of building materials was assessed using simulation techniques. It was reported that the role of emissivity is significant when the reflectivity of the materials is reduced. For high albedo values, the relative increase of emissivity offers minor advantages regarding the cooling load of buildings. Simulation results reported in (Gui et al., 2007) regarding the optical and thermophysical characteristics of paving materials concluded that both the albedo and emissivity of the materials have the highest positive impact on the surface temperature of the studied materials.

The impact of emissivity on the urban heat island is also studied in (Oke et al., 1991). Simulations showed that the role of emissivity on the heat island intensity during the night is quite minor. When the emissivity increased from 0.85 to 1.0, the temperature difference between the urban and rural environment varied by 0.4°K, and this effect was observed only for very narrow canyons.

3.2.3 The role of heat convection

Heat transfer by convection to and from the pavement surface is determined by the temperature difference between the ambient air and the pavement surface, as well as the heat transfer coefficient (hconv). Convection can be free or forced, depending on the wind speed velocity and temperature difference. According to Jiji, 2009, the free convection coefficient over a flat plate is close to 5.9 W/m²/K. For laminar air flow

and wind speeds not exceeding 2 m/s, the heat transfer coefficient can be calculated according to Çengel, 2009, while for higher wind speeds, the formula proposed in may be used.

Simulation of the heat transferred by convection from the pavements to the ambient air for Californian cities during the summer period has shown that it varies between 0.0 and 125 W/m² and is a function of the temperature difference between the materials and the ambient air. Measurements over asphalt and concrete surfaces, reported in, show that the maximum convective transfer during the hottest time of the day was 350 and 200 W/m², respectively (Asaeda et al., 1996).

3.2.4 The role of other thermal parameters

Thermal conductivity and thermal capacitance are significant parameters influencing the thermal performance of pavements. The documented thermal characteristics of pavements, particularly concrete, are well-established (Chung and Shin, 2008). Increased thermal conductivity of paving surfaces facilitates faster heat transfer between the pavements and the ground. Consequently, during daytime, when pavement temperatures surpass ground temperatures, heat is transferred to the ground, and vice versa during nighttime. Materials with higher conductivity exhibit lower average maximum temperatures and higher average minimum temperatures.

Simulations conducted in (Gavin et al., 2007) to explore the impact of thermal conductivity on pavement surfaces have demonstrated that an increase in conductivity from 0.60 to 2.60 W/m/K results in a decrease of approximately 7°K in average maximum surface temperature, while the average minimum temperature increases by 4.5°K. Another study (Hermansson, 2004) , conducted under lower solar radiation and pavement surface temperatures, concluded that the role of conductivity is marginal for pavement temperature near its surface.

Similarly, thermal capacity, or the ability of paving materials to store heat, has a comparable impact on maximum and minimum surface temperatures. Higher thermal capacity decreases the average maximum surface temperature while concurrently increasing the average minimum temperature. Simulations reported in (Gavin et al., 2007), aimed at investigating the impact of thermal capacity, revealed that an increase in its value from 1.40 to 2.80×10^6 J m^{-3} 1C^{-1} results in an almost 5°K decrease in average maximum temperature, with a substantial influence on the corresponding minimum temperature.

3.2.5 The impact of permeability

Permeable pavements allow water to pass through the voids or pores in the material, and when the material temperature increases, the water evaporates, contributing to a lower pavement surface temperature. The extent of evaporation depends on the moisture content in the material and the atmosphere, with a significant reliance on the material temperature. Higher moisture contents and increased watering can help maintain a cooler surface for permeable pavements (Yamagata, 2008). Experiments detailed in demonstrated that dry permeable pavements exhibit higher surface temperatures compared to their non-permeable counterparts (Haselbach, 2009).

However, other experimental investigations indicated that there is no discernible correlation between surface temperature and the permeability of water-retentive concrete blocks. Permeable pavements are more suitable for warm and humid climates, where rainwater is primarily utilized to cool down the pavement surface. In contrast, for dry climates where water availability is a challenge, permeable pavements may not be as suitable as a solution (Karasawa et al., 2006).

3.3 Generation of UHI

UHI is a multifaceted phenomenon influenced by a myriad of factors, broadly categorized as controllable and uncontrollable, as illustrated in Fig. 3.1 (Giridharan et al., 2004). These factors can be further classified into temporary, permanent, and cyclic variables, each playing a distinctive role in shaping UHI.

The heat within an area emanates from solar radiations and anthropogenic sources, including power plants, vehicles, air-conditioners, and mechanical equipment (Giridharan et al., 2004). Anthropogenic heat swiftly enters the environment, while solar radiations, absorbed by intricate urban structures, indirectly heat up the surroundings. Fundamental heat transfer processes—conduction, convection, and radiation—orchestrate the intricate exchange of heat.

Structures at ground level, such as walls, roofs, gardens, lawns, and paved areas, capture solar radiation to varying extents (Giridharan et al., 2004). These structures accumulate and store this radiation as heat energy from sunrise until late afternoon. The subsequent cooling of the environment prompts the release of stored heat energy from these structures. The efficiency of heat release hinges on controllable factors like the sky view factor and building material. In urban areas, the high intensity of solar radiation captured within a confined space due to massive construction materials contributes to increased heat storage. The reduced ability of urban structures to release heat through long-wave radiation, attributed to decreased sky view, results in elevated heat retention in building structures. The albedo, representing reflected light in comparison to incident light, is believed to be low in cities, especially in typical street canyon configurations, contributing to high air temperatures. Design values of albedo and sky view factor are thus identified as pivotal factors in creating UHI.

The scarcity of vegetation in cities leads to minimal latent heat of vaporization. Tokyo, for instance, experienced a 38% reduction in evapotranspiration from 1972 to 1995 (Kondoh and Nishiyama, 1999). High structural roughness in urban areas curtails convective heat removal and wind transfer. Additionally, typical thermal properties of building materials in urban areas, such as low admittance, contribute to UHI. Air pollutants, particularly abundant aerosols in polluted urban areas, absorb and re-radiate long-wave radiation, inhibiting radiative surface cooling and creating a pseudo-greenhouse effect, further contributing to UHI.

Temporary effect variables, including wind speed and cloud cover, exert notable effects on UHI. Anticyclone conditions intensify Urban Heat Island Intensity (UHII) (Pongracz et al., 2006). Various studies have reported a negative correlation between UHI and wind speed and cloud cover (Kim and Baik, 2005; Oke, 1982). Conversely, UHI exhibits a positive correlation with city population, though this

relationship varies across studies. Population density influences heat generation directly, with more people leading to increased metabolisms, and indirectly, as urban infrastructure also expands with population growth. However, factors like the sky view factor, anthropogenic heat, building design, and material play crucial roles in heat accumulation and are not solely dependent on population. Therefore, while population density might contribute to increased heat content, it is not a determining factor. Comprehensive comparisons of controllable factors and the relevant UHII across different areas could help quantify the significance of these factors and elucidate the sensitivity of individual variables on UHI. Research has begun to quantify the significance of temporary effect variables, such as wind speed and cloud cover.

For instance, Kim and Baik (2002) reported a visible decrease in maximum UHI with wind speeds greater than 0.8 m/s, and Klysik and Fortuniak (1999) found that an UHI of more than 1°C could still be observed at a city average wind speed of 4 m/s during the night and 2 m/s during the day. Morris et al., (2001) further noted that UHII is approximately the fourth root of both wind speed and cloud cover. However, more research is needed to fully understand the influence of various temporary and permanent factors on UHI (Kim and Baik, 2002; Klysik and Fortuniak, 1999; Morris et al., 2001).
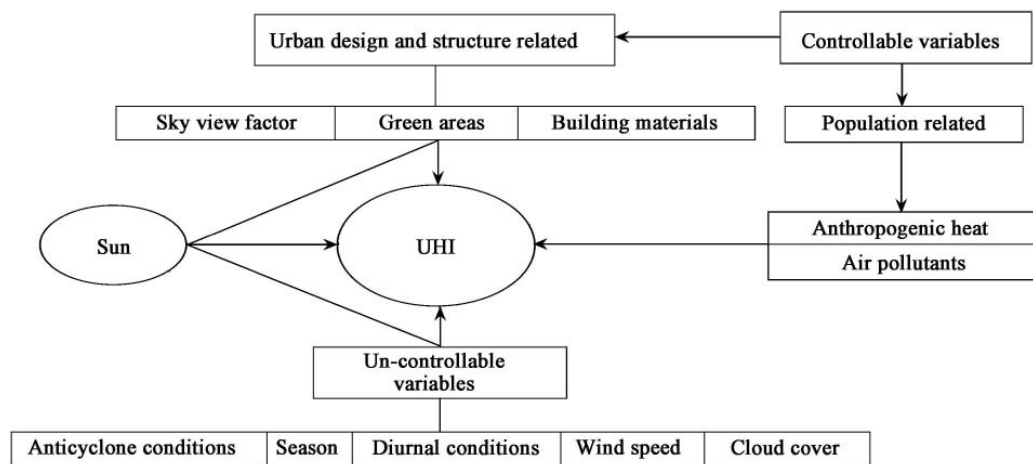
Figure. 3.1: Generation of Urban Heat Island (UHI), (Rizwan et al., 2008)

3.4 Determination of intensity

The primary objective of numerous investigations on Urban Heat Islands (UHI) is to determine their intensity during specific nights. In cases where a substantial number of observations are available, researchers seek to identify both the maximum and average intensity. The methodologies employed for this purpose vary, encompassing the comparison of two fixed observatories—one urban and the other peripheral or non-urban—utilizing mobile urban transects, or employing remote sensing

techniques.

Regardless of the chosen methodology, the core aim is to quantify the thermal disparities between contrasting points or sectors, specifically between urban and non-urban areas. The UHI intensity is essentially the temperature difference observed at a given time between the hottest sector within the city and the non-urban spaces surrounding it. This intensity serves as the most straightforward and quantitative indicator of the thermal alterations imposed by the urban environment on the surrounding territory.

It is crucial to emphasize that the intensity of the heat island is indicative of the extent of thermal modification exerted by the city on its surroundings, particularly in relation to the ambient rural environment during nighttime (Kim and Baik, 2002; Memon et al., 2009).

3.5 Cool materials

Reflective surfaces, commonly referred to as 'cool materials,' offer a cost-effective and environmentally friendly means to enhance energy efficiency in buildings. This passive technique works by reducing the energy demand for cooling and improving the overall urban microclimate through the mitigation of surface and air temperatures. The distinctive characteristics of cool materials include high solar reflectance (SR) and high infrared emittance (e).

Solar reflectance, measured on a scale of 0 to 1 (or 0–100%), gauges a material's ability to reflect solar radiation. It considers the total reflectance of a surface, encompassing both specular and diffuse reflection across the solar spectrum. On the other hand, infrared emittance, measured on a scale from 0 to 1, evaluates a surface's capacity to release absorbed heat. It quantifies how efficiently a surface radiates energy compared to a black body operating at the same temperature.

The combination of high solar reflectance and infrared emittance influences the temperature of a surface (Bretz and Akbari, 1997; Siegel and Howell 2002). When a surface with elevated solar reflectance and infrared emittance is exposed to solar radiation, it maintains a lower surface temperature compared to a similar surface with lower SR and e values. This has notable implications: for a building envelope, a cooler surface reduces the heat entering the building, and in the urban environment, it contributes to lowering the ambient air temperature due to reduced heat convection from the surface.

An illustrative example involves concrete pavement tiles, as depicted in Fig. 3.2. Tiles treated with cool coatings (1 and 4), exhibiting solar reflectance values of 0.82 and 0.83 respectively, demonstrate lower surface temperatures, as evident in the infrared image (b). Conversely, the tile treated with a black coating (SR = 0.05) experiences higher surface temperatures, emphasizing the impact of solar reflectance on surface temperature. This experimental observation, conducted under hot summer conditions in Athens, Greece, underscores the potential of cool coatings to decrease surface temperatures and contribute to overall urban heat mitigation (Synnefa et al., 2006).
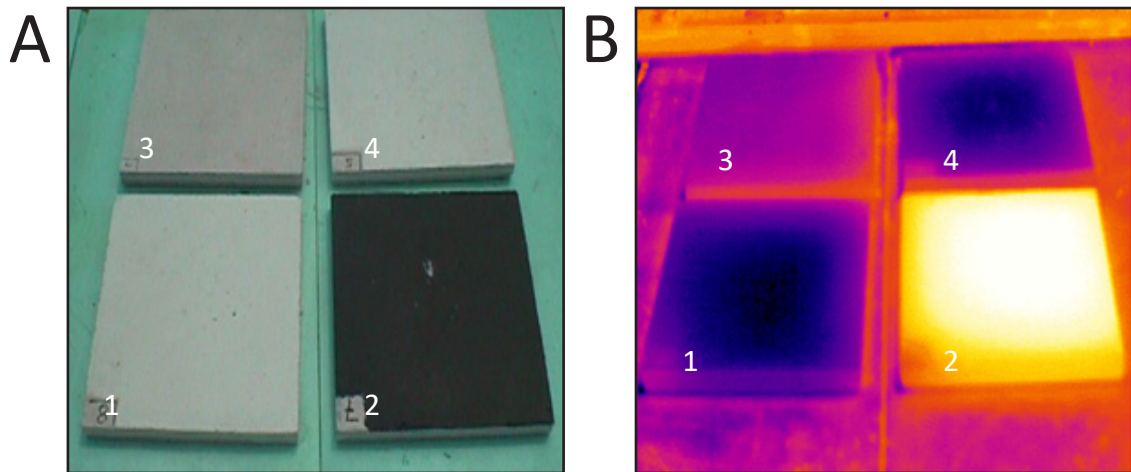
Figure 3.2: Visible (a) and infrared (b) images of four concrete tiles painted with cool white coatings (1 and 4), a black coating (2) and an unpainted off-white (3) one. The difference in solar reflectance translates into a significant difference in surface temperatures (Synnefa et al., 2006)

3.5.1 Role of cool roof

The substantial alteration of surface reflectivity, known as albedo, has been extensively recognized for its pronounced effect on local peak ambient temperatures. Notably, comprehensive observations detailed in Campra et al., (2008) reveal a significant reduction in temperature (approximately 0.3°K per decade) attributable to the extensive deployment of high-albedo greenhouses across the Almeria region in Spain. This underscores the consequential role of albedo modifications in shaping the thermal landscape.

Various simulation studies have delved into the ramifications of albedo-related mitigation techniques, with a primary focus on the potential reduction in ambient temperature. The majority of these endeavors assess the collective impact of heightened local albedo, considering a holistic approach that incorporates cool roofs, cool pavements for roadways and parking lots. However, a limited number of studies concentrate solely on the mitigating effects of reflective roofs. Concurrently, many mitigation studies explore the combined influence of diverse mitigation technologies, encompassing both increased local albedo and vegetative cover. Regrettably, these studies often present results without isolating the distinct contributions of each technique (Taha et al., 1999).

In the context of this thesis, exclusive attention is directed towards studies that either quantify the influence of reflective roofs or evaluate the cumulative impact arising from a general alteration in albedo. This selective approach aims to discern and analyze the specific effects of these distinct albedo modification strategies on ambient temperature, contributing valuable insights to the broader discourse on urban heat mitigation (Taha et al., 1999).

3.5.2 Mitigation potential of cool roofs

The exploration of cool roofs as a means to mitigate urban heat islands is a

relatively recent scientific inquiry, marked by four notable studies that delve into the potential impact of increasing roof albedo. These studies, conducted by Savio et al. (2006), Synnefa et al., 2008, Menon et al., 2010, and Jacobson and Ten Hoeve, 2012, collectively shed light on the influence of cool roofs at both local and planetary scales.

Savio et al., 2006 and Synnefa et al., 2008 focus on the local ramifications of cool roofs in New York, US, and Athens, Greece, respectively. In the New York study, simulations utilizing the Penn State/NCAR MM5 regional climate model were conducted during three heat waves in the summer of 2002. The application of cool roofs, with an average solar reflectivity of 0.5, resulted in a daily average temperature decrease ranging from 0.18°K to 0.36°K across different city areas. Similarly, peak ambient temperatures at 3 PM exhibited reductions between 0.31°K and 0.62°K.

In the Athens study by Synnefa et al., 2008, the MM5 climate model was employed to simulate the climatic impact of cool roofs on August 15, 2005. Two albedo scenarios were considered: a moderate increase from 0.18 to 0.63 and an extreme increase to 0.85. For the moderate scenario, ambient temperature decreased by 0.5°K to 1.5°K at 2 m height at 12:00 LST, while the extreme scenario resulted in reductions between 1°K and 2.2°K. The temperature decrease commenced at 9:00 LST and concluded around 20:00 LST.

Menon et al., 2010 extended the scope to a global perspective, utilizing the GATOR–GCMOM model. They increased the solar albedo of all roofs from 0.12 to 0.65, corresponding to a universal urban albedo rise of 0.147. The study suggested that a worldwide adoption of cool roofs could decrease populated weighted temperatures by 0.02°K but increase the overall earth temperature by 0.07°K. However, these findings have sparked debates and concerns, as discussed in Oleson et al., 2008, regarding assumptions and outcomes.

Similarly, another global simulation study conducted by Menon et al., (2010) employed the urban canyon model CLMU coupled with other models. Assuming a roof albedo increase to 0.9, the study indicated a daily maximum urban temperature decrease of 0.6°K and a daily minimum ambient temperature decrease of 0.3°K, resulting in an overall reduction of the urban diurnal temperature range by 0.3°K.

3.5.3 Increasing the albedo of cities-mitigation potentials

In one of the earliest examinations of the climatic consequences of reflective surfaces, Sailor, 1995 conducted a study focusing on Los Angeles, USA. Using the Colorado State University Mesoscale Model, the authors assumed a 0.14 increase in the albedo of downtown surfaces and approximately 0.08 for the entire basin. The outcomes indicated a reduction in ambient temperatures by at least 0.5°K across the majority of the area, with a noteworthy peak reduction of 1.4°K near downtown LA.

A subsequent investigation in Los Angeles by Rosenfeld et al., 1995 employed the same modeling approach. The study considered an average albedo increase of 0.13, ranging from 0.13 to 0.26 over an area of 100,000 km², where over 20% of the land was covered by artificial surfaces. For flat roofs, albedo changed from 0.25 to 0.75, and for sloped roofs, it varied from 0.25 to 0.6. The study projected a peak impact of

the albedo change in the early afternoon, resulting in a potential cooling exceeding 3°K at 3 pm. Simulations under different conditions suggested peak summertime temperature reductions between 2 and 4°K.

Continuing their research in Los Angeles, Rosenfeld et al., 1998 evaluated the cooling potential of potential albedo changes. The study involved increasing the albedo by 0.35 over almost 1250 km² of roof surface (from 0.15 to 0.5) and by 0.25 over 1250 km² of pavements (from 0.05 to 0.30). The calculated temperature reduction during the peak period approached 1.5°K, accompanied by significant estimated benefits in energy and pollution reduction.

In a broader examination of American cities, Millstein and Menon, 2011 utilized the Weather Research and Forecasting model. The study considered cool roofs and cool pavements, assuming that roofs and pavements represented 25% and 35% of the urban area, respectively. The considered albedo increase for roofs and pavements were +0.25 and +0.15, contributing to an average albedo increase for the entire area ranging between 0.0 and 0.115. Calculations suggested that cool roofs and cool pavements could contribute to a decrease in average afternoon summertime temperatures by 0.11–0.53°K, although not all urban locations exhibited statistically significant temperature reductions.

Simulations in Philadelphia, USA, conducted by Sailor et al., 2002 using the mesoscale model MM5 indicated that a local albedo increase of 0.1 could lead to an average daytime ambient temperature depression of about 0.3–0.5°K.

Zhou and Shepherd, 2010 explored the impact of various mitigation technologies in Atlanta, USA, utilizing the Weather Research and Forecasting WRF-NOAH land surface model. They found that a 100% increase in local albedo (from 0.15 to 0.30) resulted in almost negligible ambient temperature depression, but a 200% increase (to 0.45) led to a significant peak ambient temperature decrease of 2.5°K.

A study by Taha, 2008 investigated the impact of a moderate increase in local albedo in Houston, USA, using the mesoscale model MM5. Changes in roof albedo from 0.1 to 0.3, wall albedo from 0.25 to 0.3, and paved surface albedo from 0.08 to 0.2 were considered. The results indicated that the change in albedo could decrease peak temperatures up to 3.5°K, with occasional increases of up to 1.5°K. The average temperature reduction varied between 0.3 and 0.4°K in residential urban areas, occurring during daytime and resulting in nighttime heating.

Lynn et al., 2009 conducted simulations to assess the impact of various mitigation techniques in the Metropolitan New York Area, USA. Utilizing the MM5 mesoscale simulation model, the study considered an increase in the albedo of impervious surfaces from 0.15 to 0.5. Peak ambient temperature at 2 m height for 12:00 LST on August 14, 2001, decreased between 0.25 and 0.5°K, with a daily average temperature decrease close to 0.2–0.3°K.

Taha, 2008 performed simulation studies to investigate the impact of various mitigation techniques in several cities of California, USA, using the PSU/NCAR MM5 simulation tool. Two scenarios related to albedo change were considered, involving a moderate increase in urban reflectivity and a stronger increase. Albedos ranged from 0.117 to 0.152 for the existing situation, from 0.18 to 0.252 for the moderate albedo

change scenario, and from 0.199 to 0.374 for the last scenario. The study found that a moderate change in urban albedo may decrease peak ambient temperatures by up to 1°K, while a stronger change contributes to a decrease of up to 2°K.

In summary, these studies collectively span various cities and scenarios, revealing a potential increase in urban albedo ranging between 0.01 and 0.35. The calculated decrease in average ambient temperature ranges from 0.0 to 1.0°K, with a variation of 0.0 to 0.61°K in average ambient temperature per 0.1 albedo change. The relationship between albedo change and average temperature decrease is reasonably well captured by a linear regression model, as expressed in Equation (1), where a is approximately 3.11 and R^2 is 0.85. This regression model provides valuable insights into the relationship between albedo change and its corresponding impact on average ambient temperature.

ATD = αALBIN

Furthermore, the calculated reduction in peak ambient temperature varies between 1 and 3.5°K, with an estimated decrease per 0.1 albedo change ranging from 0.57 to 2.3°K. Despite the data's scattered nature, a linear relation between albedo change and the decrease in peak ambient temperature has been established, emphasizing that a 0.1 albedo change in urban areas may result in a substantial decrease of approximately 0.9°K.

3.6 Mitigation potential of green roofs

Limited studies have sought to assess the potential of green roofs in mitigating the urban heat island effect on a city scale. These investigations primarily rely on simulation techniques, predominantly utilizing mesoscale models, and often focus on extensive roof types. Notable studies have been conducted in cities such as New York and Chicago in the United States, as well as Hong Kong and Tokyo. An additional experimental study in Singapore contributes valuable insights.

Smith and Roeber, 2011 conducted a simulation study in Chicago, a city at the forefront of green roof technology. Utilizing the Advanced Research version of the Weather Research and Forecasting Model coupled with an urban canopy model, green roofs were simulated with an equivalent albedo of 0.8, based on findings by Rosenzweig et al., 2006. The results indicated a significant cooling effect, with urban temperatures during 19:00–23:00 being 2–3°K cooler compared to simulations without green roofs.

A comprehensive study on heat island mitigation techniques in New York Savio et al., 2006 included simulations assessing the impact of extensive grass-covered roofs. The study reported a decrease in peak ambient temperature at 2 m height during 12:00 LST on August 14, 2001, ranging from 0.37 to 0.86°K. The daily average temperature decrease was approximately 0.3–0.55°K.

In Tokyo, simulations evaluating various mitigation techniques, including green roofs, were conducted using the CSCRC model Chen et al., 2009. The study considered extensive roofs planted with grass and concluded that the installation of vegetative roofs in medium and high-rise buildings had a nearly negligible potential to decrease ambient temperature at street level.

Similar results were observed in Hong Kong by Ng et al., 2012, where simulations using the EnviMet tool evaluated the climatic impact of vegetative roofs in high-rise buildings. Enviment is a software capable of doing holistic three-dimensional model used to simulate the interaction between built-up areas, urban vegetation, and the air. Both intensive and extensive green roofs were simulated, and the study found that the potential decrease in ambient temperature at street level in this high-rise, high-density area was almost zero. The study suggested that the cooling benefits at ground level are low when the building height to street width ratio exceeds 1.

Measuring the ambient air temperature over vegetated and conventional roofs in Singapore, Wong et al., 2003 reported that the cooling effect of vegetative roofs was constrained by distance from the roof. The study found a maximum temperature difference of 4.2°K at 30 cm from the roof at 18:00 h, emphasizing that green roofs may be more effective when the building height is lower than 10 m.

Sun et al., 2012 conducted a similar experimental study in Taipei, measuring ambient temperatures over a green roof and at a height of 2.5 m. The study reported an average decrease of 0.26 °C and a maximum temperature decrease close to 1.6°K. Unlike Wong et al., 2003, Sun et al., 2012 found that the influence of green roofs was more pronounced during the daytime.

In summary, the collective findings from these mitigation studies, as outlined in Table 3, underscore that the potential of vegetative roofs is nearly negligible when installed in high or medium-rise buildings. Noteworthy differences exist between the reported results for Chicago and New York, with the calculated mitigation potential in Chicago being almost 2–3 times higher (2–3°K) than that in New York (0.3–0.86°K). It is crucial to note that the Chicago study indirectly simulated the impact of green roofs by neglecting latent phenomena and employing an equivalent albedo, akin to a cool roof.

3.6.1 Park and green areas

According to Shashua-Bar and Hoffman, 2000, the combination of evapotranspiration and shading in parks and green areas leads to a significant decrease in temperature, creating what is known as cool islands within the city. Several studies have examined temperatures in parks and beneath trees, consistently finding that green spaces are cooler than areas lacking greenery. Eliasson, 1996 demonstrated that the mean air temperature difference between a park and the city center could be as high as 4°C.

Examining temperature variations not only in green spaces but also in the surrounding commercial areas, Yuan and Hien, 2006 discovered significant cooling effects of green spaces in Singapore. The results indicated that vegetation not only in parks but also in the nearby urban zones could yield energy savings and reduce the cooling load of buildings by up to 10%.

In a field study conducted by Cao et al., 1998 in Tama, New York, a coastal city in the Tokyo metropolitan area, the researchers collected data to quantify the impact of a park on the summer climate in the nearby area. The study analyzed ways to reduce energy consumption for air conditioning, measuring air temperature, relative

humidity, and other meteorological factors at various locations within the park and neighboring areas. The results showed that vegetation significantly modified the city's climate, with a temperature reduction of up to 1.5°C in a busy commercial area 1 km downwind at noon. This led to a noteworthy decrease in cooling energy consumption in the commercial area.

The overall findings from these studies suggest that parks and green spaces can play a crucial role in mitigating urban heat island effects and reducing cooling energy consumption in summer. Additionally, these green spaces contribute to stabilizing temperature fluctuations caused by building materials Yu and Hien, 2006. However, the exact mechanisms through which parks affect the formation of the heat island were not entirely clear. The cooling effects appeared to depend on the size of the park and seasonal radiation conditions, with no linear relationship between park size and the intensity of the cool island. The intensity was primarily determined by the area occupied by trees and shrubbery in the park, as well as the park's shape, with grass having a negative impact on cool island formation.

To better understand and predict the intensity of cool islands in parks, Cao et al., 2010 proposed a Park Vegetation and Shape Index (PVSI). This index could assist urban planners in designing cooler parks that counteract the effects of the urban heat island.

3.6.2 Trees and vegetation

Several studies have investigated the impact of vegetation and tree shade on reducing energy consumption in buildings (Rosenfeld et al., 1995). Robitu et al. found that a significant cooling effect from vegetation could lead to energy savings of up to 10% in cooling buildings, with an estimated temperature reduction of 3–5°C (Robitu et al., 2006). Akbari et al., 2005 monitored power peaks and energy savings in cooling produced by tree shade in houses in Sacramento, California. Shading trees resulted in seasonal cooling energy savings of 30%, equivalent to mean average daily savings of 3.6 and 8 kWh/d. The shade from trees effectively reduced the temperature of outer building surfaces as effectively as wind speed.

Other researchers have delved into the influence of greenery on building design and urban planning (Guhathakurta and Gober, 2007). Ong proposed a novel architecture metric called the Green Plot Ratio (GPR), aiming to determine optimal green plot ratios for different land uses and provide guidelines for development. The proposed Leaf Area Index (LAI) values, ranging from 1.36 to 10 for lawns, shrubs, and full-grown trees with a dense canopy, were suggested to compensate for the loss of green spaces due to urban development. According to Ong, the Green Plot Ratio is an effective tool for facilitating sustainable urban development (Ong BL, 2005).

Wong et al., 2011 conducted simulations on the effects of vertical greenery systems on building temperature and energy consumption. They discovered that 100% greenery coverage from vertical greenery systems effectively lowered the mean radiant temperature of a glass facade building. Additionally, a lower shading coefficient led to greater thermal insulation. A 50% greenery coverage

with a shading coefficient of 0.041 reduced the envelope thermal transfer value (ETTV) of a glass facade by 40.68%, significantly lowering the energy cooling load. Increased greenery coverage also contributed to a drop in the minimum estate air temperature over a large region.

However, it's essential to note that the presence of vegetation can also have negative effects on the urban microclimate in cold climates. McPherson et al., 2009 used computer simulations to analyze the impact of vegetation on space heating and cooling in four representative U.S. cities with different climates. In cold climates, dense shade, such as that provided by conifers, increased heating costs up to 21%. On the other hand, in cities with temperate and hot climates, dense shade on all surfaces reduced annual space cooling costs by 53–61% and peak cooling loads by 32–49%. Wind reductions were found to be beneficial in cold climates but could be counterproductive in more temperate climates if vegetation was not strategically placed.

In summary, these studies collectively affirm that site climate, tree species, and the number of trees relative to surface area are critical factors influencing the energy consumption of nearby buildings. It emphasizes the need for a nuanced understanding of the interplay between vegetation and local climate for effective urban planning and energy conservation.

4. Methodology

In this part of the thesis, the researched area, natural green areas and land cover as a whole, which characterize the distribution of urban areas, are briefly described as a map. The chapter also describes the Urban Atlas2018 input data (Copernicus, 2023), heat wave transition data from the MUKLIMO_3 model and surface temperature data obtained from Google Earth Engine (GEE) satellite images used in the discussion. For clarity, the area of interest was overlaid with the Urban Atlas 2018 layer (hereafter referred to as UA2018), which divided the Prague 3 into a segment of 600 x 600 m in size, and a segment is assigned one of the UA2018 classes. There are 45 of them in total, but in this work only 3 main layers will be monitored (see figure no. 4.1).

Using the reclassification function in the ArcGIS application, so-called thermally stressed areas where the air or surface temperature exceeded 30 °C were selected from the temperature layers. The resulting layers of thermally stressed areas were connected to the UA2018 layer in order to analyze the connections between land use class and temperature characteristics.

Altitude is also important for the development of air temperature and surface temperature. Therefore, the individual temperature data (MUKLIMO_3 and data obtained from GEE) were supported by a layer of shaded relief, and by connecting the attribute tables, map outputs were created showing the distribution of thermally stressed areas (in terms of air and surface temperature) in relation to altitude (see appendices no. 1 and 24).

For a more comprehensible interpretation of the results, tables and graphs were generated that show the representation of individual classes of land use and the frequency of occurrence of temperatures exceeding 30 °C, which are formulated in the results as thermally stressed areas.

Most of the work was done on the GIS platform.

4.1 Case Study and Monitored characteristics

Among the observed characteristics in the thesis is mainly the air temperature. This characteristic will be analyzed with respect to the type of land use UA2018. This creates an imaginary network and examines the viability of implementing green roofs at a precinct scale in Prague 3, Žižkov with a cell size of 600 x 600 m, where each cell will contain attributes that represent temperature data and the type of use of the given territory. This characteristic is necessary for the other goals of the work, which is to obtain a connection between individual surfaces.

4.1.1 Czech Republic, Prague

The Czech Republic and its capital, Prague, have experienced a rising occurrence of extreme weather events linked to climate change over the past few decades. The average annual air temperatures have been steadily increasing at a rate of approximately 0.3°C per decade. Projections indicate a further 1°C increase by 2030 across the Czech Republic (IPR Praha, 2020).
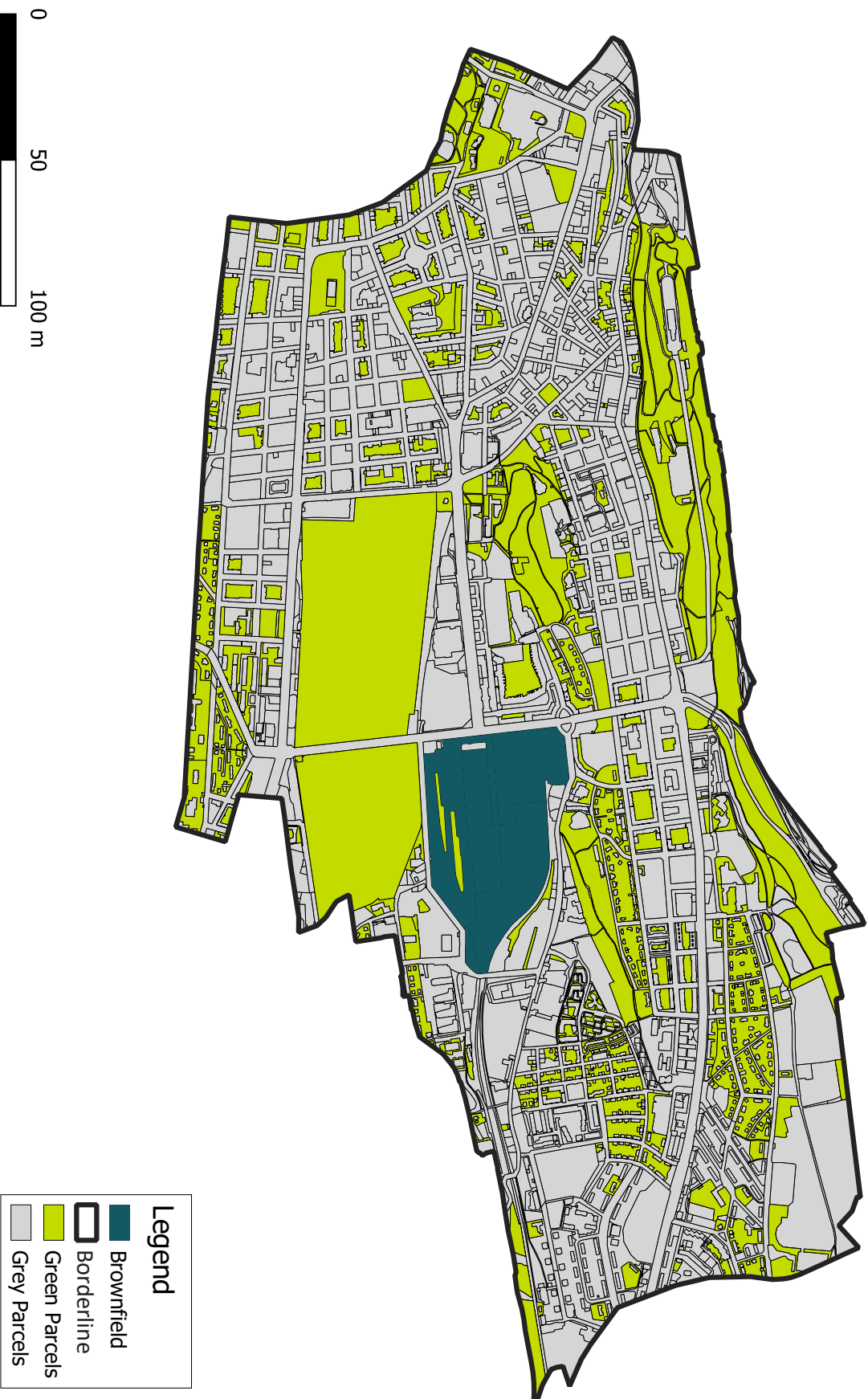
Green VS Grey Parcels, Prague 3

Figure. 4.1: Diversification of green parcels and grey ones in Prague 3, (Geoportal Praha, 2024)

Legend
- Brownfield
- Borderline
- Green Parcels
- Grey Parcels

0   50   100 m

Prague, in particular, faces an anticipated rise in the frequency, intensity, and duration of extremely hot periods, commonly known as heat waves. Additionally, changes in the hydrological cycle and rainfall patterns over time and space pose new challenges. There is an escalating risk of torrential rains leading to local floods, as well as fluctuation in discharge levels, alternating between droughts and floods. Winter precipitation is expected to rise, while summer precipitation will likely decrease. The number of days without precipitation is also expected to significantly increase, along with the risk of droughts. Climate models predict a heightened frequency of extreme weather events such as windstorms and tornados.

To address these challenges, the Capital City of Prague has developed a Climate Change Adaptation Strategy aligned with the national Strategy on Adaptation to Climate Change, endorsed by the Czech Republic Government in 2015 (Prague City Hall, 2020). The primary focus is on employing nature-based solutions, utilizing green and blue infrastructures. These solutions involve natural vegetation patterns that cool the environment through evaporation and provide shade. Moreover, they aid in capturing, retaining, and infiltrating rainfall into soil layers or underground water (IPR Praha, 2020).

The Adaptation Strategy also emphasizes the conservation of water, soil, and biological components of the natural landscape. It aims to protect and restore ecosystems resilient to climate change, contributing to the prevention of natural disasters through an ecosystem-based approach or nature-based solutions.

In cases where nature-based solutions are impractical, the strategy advocates the use of suitable technological (grey) and soft measures. Examples of soft measures include early warning systems, communication strategies, education, and public awareness campaigns, and examples of grey ones are the use of technology in grey parcels such as building, infrastructure, and man-made structures .

This strategy tries to take into account specific Capital City of Prague´s patterns as the urban landscape, being characterized by high proportion of built-up areas, economic, technological and transport infrastructure high accumulation and unevenly dispersed vegetation component distribution. The Capital City of Prague, by joining the Mayors Adapt Initiative, has committed to developing a climate change adaptation strategy. This involves monitoring and assessing the adaptation measures, including risk assessment and the formulation of biennial assessment reports. These reports outline specific adaptation measures and pilot projects contributing to climate change mitigation, with ongoing monitoring and evaluation of their effectiveness (Prague City Hall, 2020).

Prague experiences a temperate climate with characteristics of both oceanic and humid continental climates. Winters are moderately cold, with average lows reaching -4°C and limited sunshine. Snowfall typically occurs between mid-November and late March, though significant accumulations exceeding 20 cm are uncommon. Occasional warm spells may interrupt the winter season. Summers are generally sunny, with average highs of 24°C. Rainfall is prevalent throughout

the year, even during the driest months, February. (Prague Climate: Weather Prague & Temperature by Month, n.d.).

4.1.2 Study Area, Prague 3

The current Žižkov district, had its beginnings as sparsely populated countryside on the outskirts of Prague (Figure 4.2). This transformation began in 1358 with Emperor Charles IV's decree to establish vineyards encircling the city within a three-mile radius. Residents of these newly formed "hory viniční," or "vineyard hills," enjoyed special privileges, including tax exemptions, fostering a unique viticultural community. The village of Hory Viničné, documented in 1788, stood as the heart of this flourishing era, nestled on the slopes of Vitkov Hill. While other settlements like Hrabovka and Ohrada lost their previous value as they had before. An 1837 census paints a picture of the district (encompassing both Žižkov and Vinohrady) as primarily rural, with only 66 houses and estates housing 169 inhabitants and their 216 head of livestock (IPR Praha, 2020).

One worthy part to mention about this region is that after the devastating plague outbreak in Prague, there was a need to build burial grounds and cemeteries outside of city walls. Therefore, today the majority of the green parcels in this region are mainly cemeteries, which has been remained since then.

4.2 Data processing

The main database to analyze and process the denoted issue concerning urban heat island effect are from *USGC* and *IPR Praha* in which Esri ArcGIS pro is utilized for the process (IPR Praha, 2020; USGC, 2024). The Microsoft Excel program is used to create the graphs necessary for data classification. The resulting processed data are in the form of attribute tables, graphs, spatial analyzes or otherwise edited data.

The work will process surface temperatures from Landsat 8 satellite images through the web application Google Earth Engine, which will be further processed by the ArcMap application and used in the discussion. Furthermore, historical air temperature data from Libuš and Ruzyně stations are subjected to analysis and will be compared with the measured values from the previous step in order to illuminate the variation of Surface heat island effect in the region . The underlying data which are included, for example, the UA2018 layer (Copernicus, 2023), or the layer showing the height above sea level in the form of WMS (Shaded relief model) available on the website of the geoportal of the Czech Land Surveying and Cadastral Office (ČÚZK, 2023).

The input data (see appendices no. 1 to no. 24) will be modified using ArcMap tools for spatial analysis, specifically by reclassification (required for changing input values in grids), raster calculator (for calculation of individual reclassified data), unification (which unifies multiple input layers , without changing the shape of the original data) and summarization (summarization of data from attribute tables of values are used for statistical evaluation according to the required criteria. For the purposes of the work, it was necessary to divide the data into maximum, minimum and average
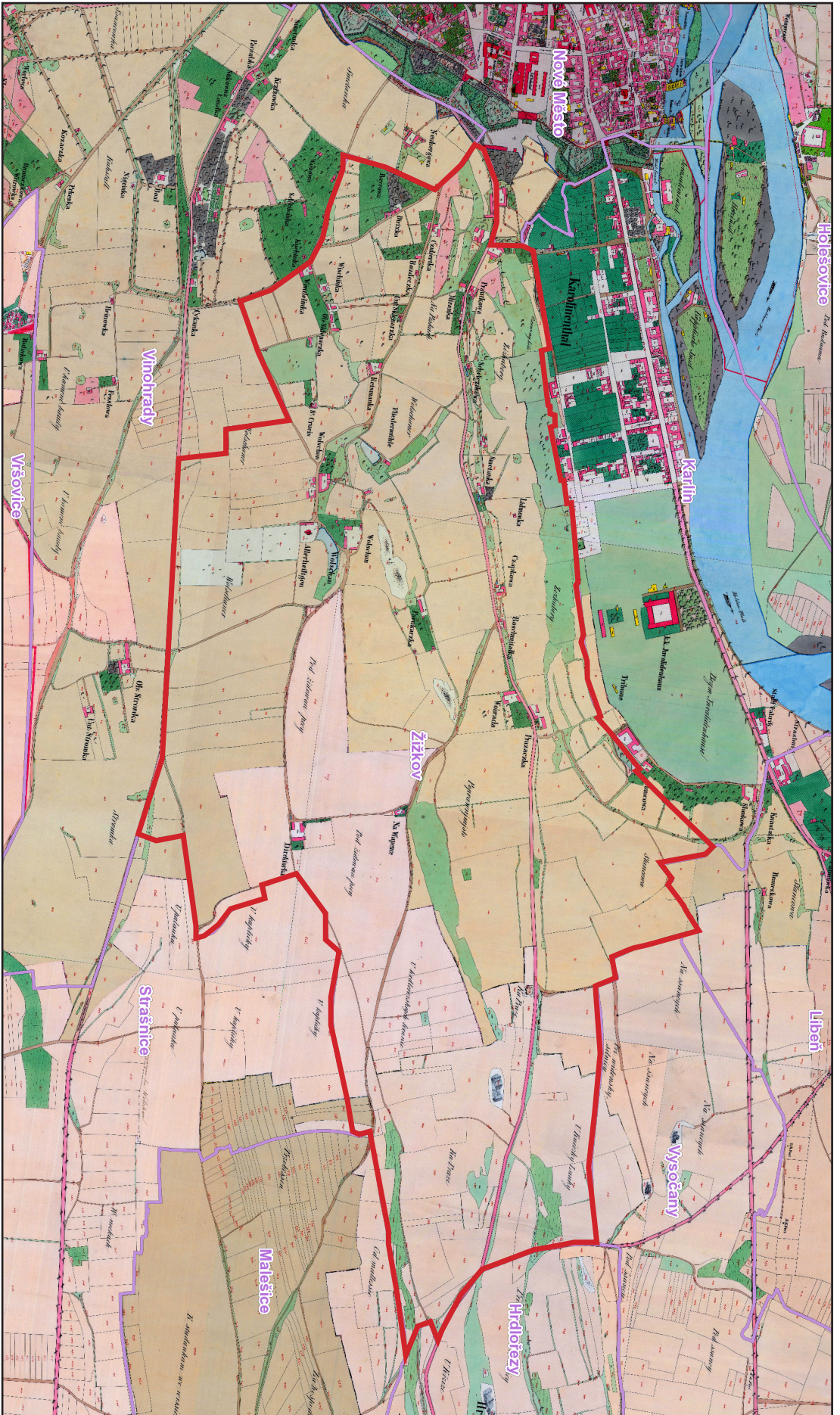
Figure. 4.2: Historic map of Prague 3,18th Century (Geoportal Praha, 2024)

values). Subsequently, these stimulated data of the heat wave over Prague is divided into intervals according to the critical limit temperature of 30 °C, which is the border between the temperature norm and the tropical day temperature (The phenomenon which weather does not drop below 30 °C during day time). This step is used to sort stressed places in Prague, where the temperature exceeded the limit set by the processor, i.e. 30 °C. The resulting layers of the spatial distribution of air temperature and surface temperature during the transition of the heat wave were subsequently combined with the layers of land use, land cover and altitude in the territory of Prague. This made it possible to compare the connection between temperature characteristics and surface properties. The specific processing of individual data is described in the following subsections.

4.2.1 Heat wave transition data

The data from Geoportal praha, 2022 describe the course of the air temperature in Prague during 30 July 2022 in hourly intervals with a spatial resolution of approximately 100m. The selected day was the warmest day of the heat wave lasting until 30th of July. The average, minimum and maximum temperature at the Prague–Ruzyně station on this day was (Average: 23.3 °C, minimum: 14.5 °C and maximum: 31.6 °C) (ČHMÚ, 2023).

The MUKLIMO_3 models the three-dimensional field of wind, temperature and air humidity using a horizontal grid. For more accurate modeling of the development of meteorological elements, the model includes the parameterization of urban surfaces. Urban areas are considered a porous medium in which pores represent the space between buildings. The MUKLIMO_3 model forms a description of construction activities with at least 13 classes, which are described by the proportion of floor area of buildings, the height of buildings and the proportion of closed and green areas between individual buildings. These classes also include undeveloped classes such as forest, park, open spaces and others. Other input data taken from the MUKLIMO_3 model can be viewed in raw form in Annexes No. 1 to Annex No. 24 (DWD, 2023).

Input data from the MUKLIMO_3 model was exported at hourly intervals for one full day. By reclassifying these hourly grids according to individual values, the necessary output data for further evaluation is achieved. All data were converted into one layer, where the key value for data classification is the temperature limit of 30 °C, which is also the temperature limit for a tropical day. This identified areas where the temperature exceeded 30 °C. Based on this, the most thermally stressed areas of Prague were determined. Subsequently, this output is connected by spatial methods to the UA2018 layer. With this step, it is possible to find out on which surfaces the temperature exceeded 30 °C and for how long (1-8 hours), which can indicate the ability of individual types of surfaces to effectively reduce/increase the thermal load of their surroundings (Figure 4.3).

A partial task was to convert the data from ASCII format to a polygon layer for further processing and for compatibility with other input layers. By subsequent connection with the UA2018 layer, an output is achieved that unites areas where

the air temperature exceeded the 30 °C limit. These areas are separately selected by summarization procedures. Here, the temperature data remained complete, in contrast to the previous modifications, so we can monitor for each pixel (100 m) the use of the area and its specific minimum, average and maximum temperature. In this way, the connection of individual surfaces to air temperature and the type of land use can be monitored. More closely identified results from air temperature data processing can be found in Chapter 5 – Results.
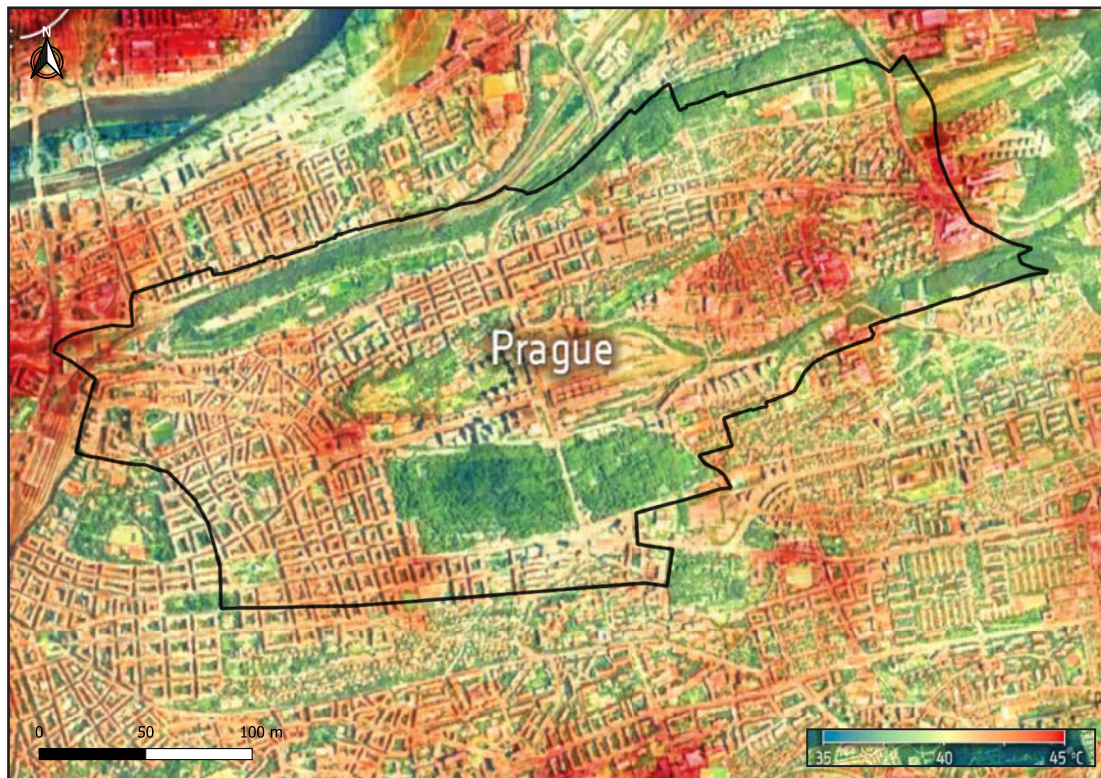

Figure. 4.3: Land-surface temperature in Prague

4.2.2 Data from the Landsat 8 satellite

Landsat 8 data representing surface temperature and used to compare the type of land use and the temperature in individual areas of Prague. Map output for input data to the analysis (to be viewed in Appendix No. 24).

For the analysis of the spatial distribution of the surface temperature, the average of three Landsat 8 images (from the period June 2022–August 2022) obtained using Google Earth Engine was used. The archive includes MODIS, Sentinel and Landsat images. Its main advantage is the software independence of the user, HPC (High Performance Computing) functions are used for data processing, which ensures fast access to the necessary data and obtaining the necessary data from the GEE computer system. Sorting of data takes place directly in the dialog window of the web browser. This requires the writing of an algorithm that serves to obtain the basic characteristics of the required data.

The first step to obtain data is to define the area of interest, which is Prague 3. For the reliability and usability of the images, it is necessary to set the detection algorithm for

clouds, which could invalidate the ascending data. By setting the spectral bands in the code, the data was divided into the smallest and the highest value (Figure no. 4.4). For reliable classification of data, the same time period during which data was collected from the MUKLIMO_3 model was chosen (for data variability, 28 a wider time period, in case some degraded images passed the previous cloud filter). Therefore, the time zone from June 2022 to August 2022 is selected.

In the following lines of the algorithm (see figure no. 4.5), the values of the NDVI index, the spectral band without the need to treat the influence of the atmosphere and the calculation of the vegetation ratio and emissivity, which are necessary to obtain the desired data, were set. These steps are less important for the work and are therefore not specified here.

The resulting layer is in .tif format, which is compatible with the ArcGIS application, where its further analysis took place. The sources from GEE were, like other data, connected to the UA2018 layer for the purpose of analyzing spatial links between surface temperature and land cover type and further processed in the same way as temperature data from the MUKLIMO_3 model.

```javascript
1  //cloud mask
2  function maskL8sr(col) {
3    // Bits 3 and 5 are cloud shadow and cloud, respectively.
4    var cloudShadowBitMask = (1 << 3);
5    var cloudsBitMask = (1 << 5);
6    // Get the pixel QA band.
7    var qa = col.select('pixel_qa');
8    // Both flags should be set to zero, indicating clear conditions.
9    var mask = qa.bitwiseAnd(cloudShadowBitMask).eq(0)
10              .and(qa.bitwiseAnd(cloudsBitMask).eq(0));
11   return col.updateMask(mask);
12 }
13
14 //vis params
15 var vizParams = {
16 bands: ['B5', 'B6', 'B4'],
17 min: 0,
18 max: 4000,
19 gamma: [1, 0.9, 1.1]
20 };
21
22 var vizParams2 = {
23 bands: ['B4', 'B3', 'B2'],
24 min: 0,
25 max: 3000,
26 gamma: 1.4,
27 };
28
29 //load the collection:
30 {
31 var col = ee.ImageCollection('LANDSAT/LC08/C01/T1_SR')
32 .map(maskL8sr)
33 .filterDate('2017-06-20','2017-8-02')
```

Figure 4.4 :The first part of the algorithm, input values obtained from the LandSat 8 satellite

27

```
34   .filterBounds(geometry);
35   }
36   print(col, 'coleccion');
37
38   //imagen reduction
39 ▾ {
40   var image = col.median();
41   print(image, 'image');
42   Map.addLayer(image, vizParams2);
43   }
44
```

```
45   //median
46 ▾ {
47 ▾ var ndvi = image.normalizedDifference(['B5',
48   'B4']).rename('NDVI');
49 ▾ var ndviParams = {min: -1, max: 1, palette: ['blue', 'white',
50   'green']};
51   print(ndvi,'ndvi');
52   Map.addLayer(ndvi, ndviParams, 'ndvi');
53   }
54
55   //select thermal band 10(with brightness tempereature), no calculation
56   var thermal= image.select('B10').multiply(0.1);
57 ▾ var b10Params = {min: 291.918, max: 302.382, palette: ['blue',
58   'white', 'green']};
59   Map.addLayer(thermal, b10Params, 'thermal');
60
61   // find the min and max of NDVI
62 ▾ {
63 ▾ var min = ee.Number(ndvi.reduceRegion({
64   reducer: ee.Reducer.min(),
65   geometry: geometry,
66   scale: 30,
67   maxPixels: 1e9
68   }).values().get(0));
69   print(min, 'min');
70 ▾ var max = ee.Number(ndvi.reduceRegion({
71   reducer: ee.Reducer.max(),
72   geometry: geometry,
73   scale: 30,
74   maxPixels: 1e9
75   }).values().get(0));
76   print(max, 'max')
77   }
78
79   //fractional vegetation
80 ▾ {
81   var fv =(ndvi.subtract(min).divide(max.subtract(min))).pow(ee.Number(2)).rename('FV');
82   print(fv, 'fv');
83   Map.addLayer(fv);
84   }
85
86   //Emissivity
87
88   var a= ee.Number(0.004);
89   var b= ee.Number(0.986);
90   var EM=fv.multiply(a).add(b).rename('EMM');
91   var imageVisParam3 = {min: 0.9865619146722164, max:0.989699971371314};
92   Map.addLayer(EM, imageVisParam3,'EMM');
93
94   //LST in Celsius Degree bring -273.15
95   //NB: In Kelvin don't bring -273.15
```

Figure 4.5 :The second part of the algorithm, input values obtained from the Land-Sat 8 satellite

```
 96  var LST = thermal.expression(
 97  '(Tb/(1 + (0.00115* (Tb / 1.438))*log(Ep)))-273.15', {
 98    'Tb': thermal.select('B10'),
 99    'Ep': EM.select('EMM')
100  }).rename('LST');
101  Map.addLayer(LST, {min: 20.569706944223423, max:29.328077233404645, palette: [
102    '040274', '040281', '0502a3', '0502b8', '0502ce', '0502e6',
103    '0602ff', '235cb1', '307ef3', '269db1', '30c8e2', '32d3ef',
104    '3be285', '3ff38f', '86e26f', '3ae237', 'b5e22e', 'd6e21f',
105    'fff705', 'ffd611', 'ffb613', 'ff8b13', 'ff6e08', 'ff500d',
106    'ff0000', 'de0101', 'c21301', 'a71001', '911003'
107    ]},'LST');
108
109  Export.image.toDrive({
110    image: LST,
111    folder: 'LC8',
112    description: 'Praha3',
113    region: geometry,
114    crs: 'EPSG:3857',
115    maxPixels: 1e9
116  });
117
```

Figure 4.5 :The second part of the algorithm, input values obtained from the Land-Sat 8 satellite

5. Results

This chapter of the diploma thesis deals with the summary and classification of the resulting data. The results are visualized using tables, graphs and map outputs. The monitored factors are the number of areas approximately 100 x 100 m in size and their minimum, average and maximum temperatures. The most thermally stressed classes were identified. And the least thermally stressed classes, which from the performed analysis show the ability to break down the accumulated heat.

## 5.1 Analysis of temperature-stressed places in Prague

The analysis of temperature-stressed places in Prague during the transition of the heat wave in the summer of 2020 was processed from several input layers, as can be viewed in the Methodology chapter. The specific data were temperature data in an hourly interval from the MUKLIMO_3 model. A set of data sets consisting of temperature data, land use, and land cover from UA2018 were used. Figures 5.1 and 5.2 show the spatial distribution of temperature-stressed areas of Prague, where the air and surface temperature exceeded the 30 °C limit. Figure 5.1 shows overheated surfaces in red for Prague. The 30 °C limit was exceeded on a total area of 191.27 km2 (there were over 28,000 individual pixels), which represents approximately 38% of the area of Prague. The largest part of the affected areas are the areas of former working-class districts in the wider center of Prague, specifically Holešovice, Troja, Vysočany, and Nusle. Outside the city center, wider areas with a surface temperature are found mainly in the areas of current industrial areas (Malešice and Michle), shopping centers and warehouses (Černý Most, Horní Počernice, Letňany), transport areas (Václav Havel Airport) and some housing estates (Bohnice, Prosek, Prosek, Krč, Michle, Letňany). In the southwestern part, these are the areas: Zbraslav and Komořany.

As can be clearly seen from graph no. 5.1.1, the most represented areas where the surface temperature exceeded 30 °C are continuous urban development (with density > 80%); discontinuous dense urban development (with density between 50% and 80%); industrial, commercial and private units, but also green urban areas, arable land and pastures. As already mentioned, Figure 5.2 shows areas of Prague where the air temperature exceeded 30 °C in between Jun-Aug 2022. These areas are potentially prone to excessive overheating. An area with a total area of 97.34 km2 is represented here, which corresponds to 18.4% of the total area of Prague. From the picture, it can be determined that the most stressed areas of Prague are mainly the wider center and the southwestern part at the mouth of the Berounka River into the Vltava. Specifically, these are residential parts of the city (Dejvice, Smíchov, Staré Město, Vinohrady, Žižkov, Strašnice, Prosek, Vysočany), industrial areas (Malešice, Holešovice, Horní Počernice), traffic areas (Letňany, Kbely). In the southwestern part of the city, these are the areas: Velká Chuchle, Radotín, Zbraslav, Modřany and Komořany.
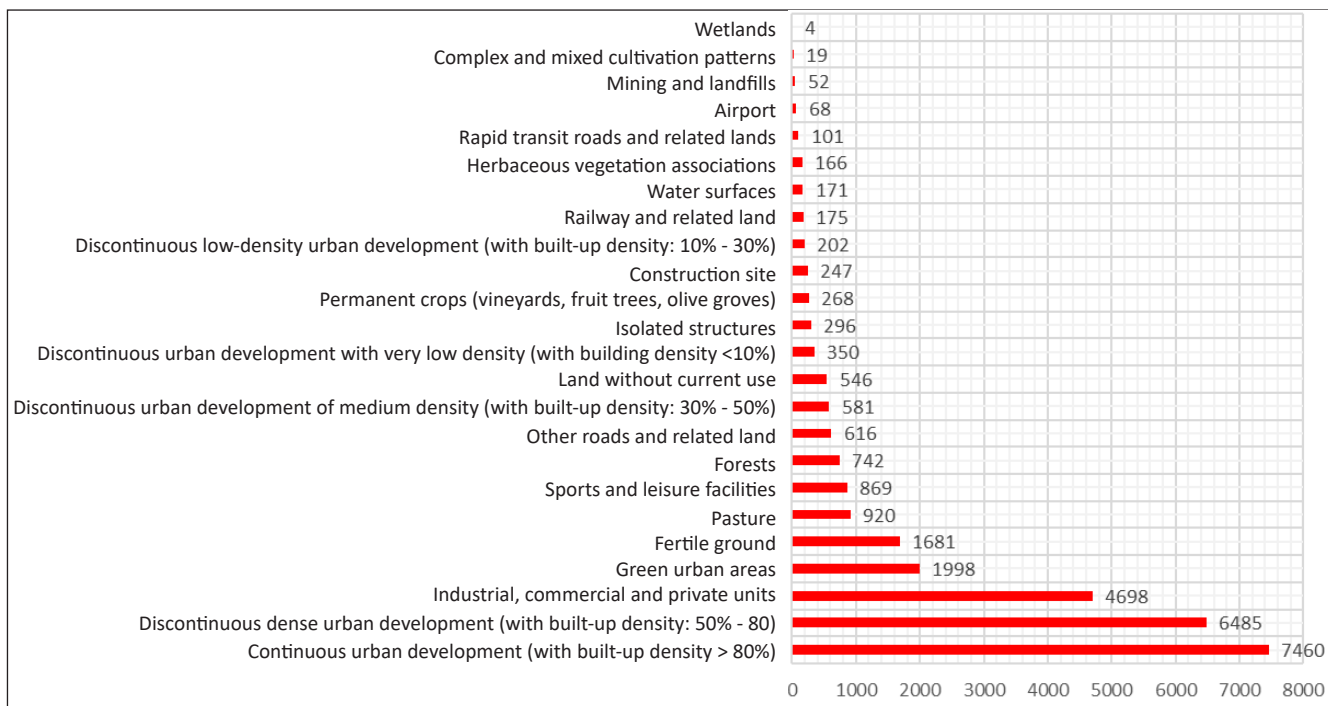
Graph 5.1.1 :The number of areas where the surface temperature exceeded 30 °C in the territory of the capital city of Prague (author).

As can be seen from graph no. 5.1.2, the most thermally stressed land use class is continuous urban development (with density > 80%); industrial, commercial and private units; other roads and related land; non-contiguous dense urban development (with density between 50% and 80%), but also green urban areas, arable land.
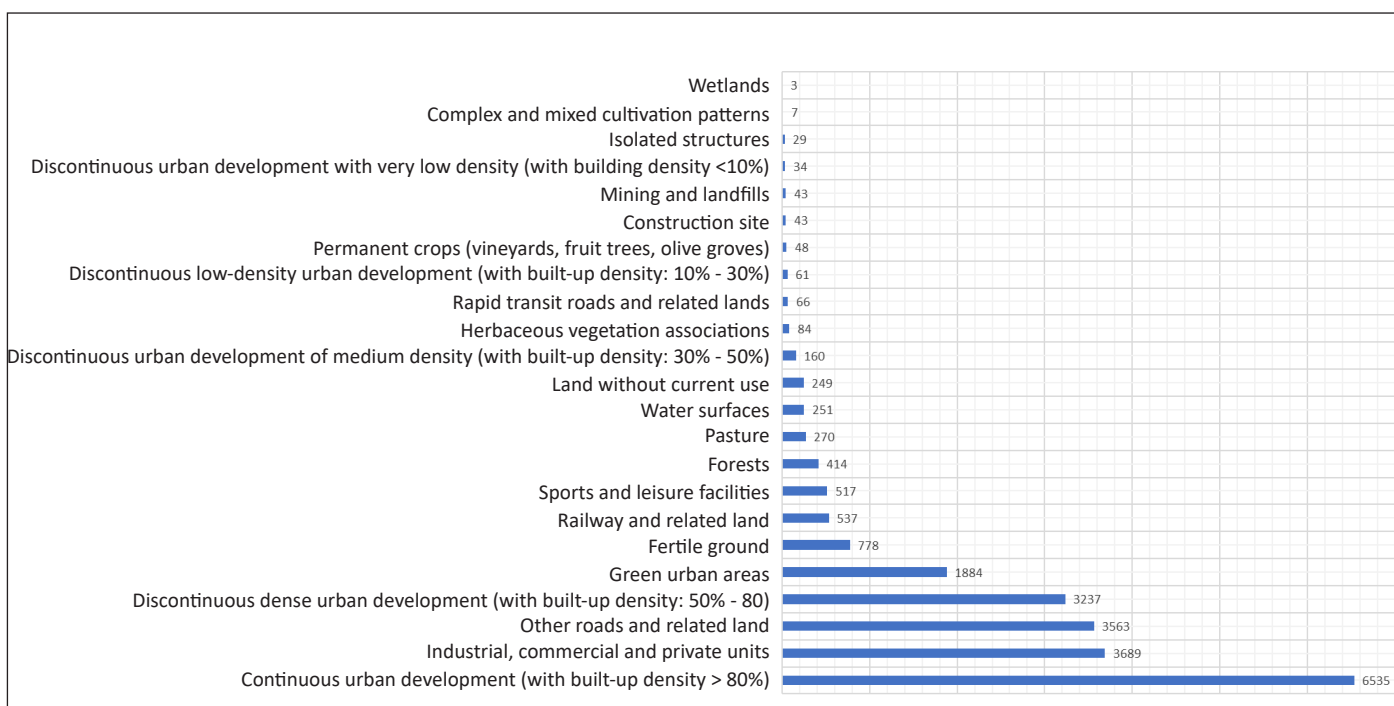
Graph 5.1.2 :The number of areas where the air temperature exceeded 30 °C in the territory of the capital city of Prague (author).
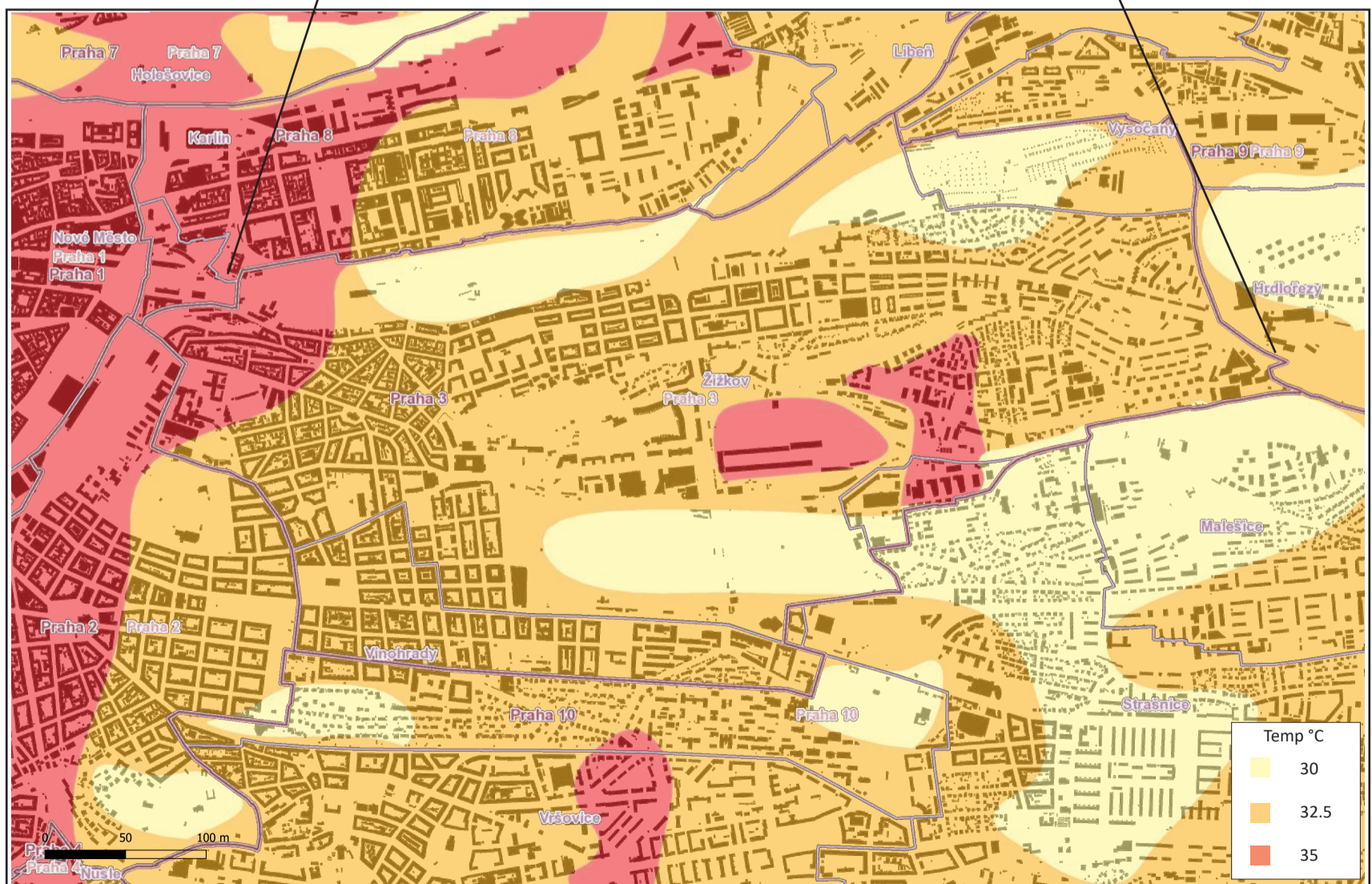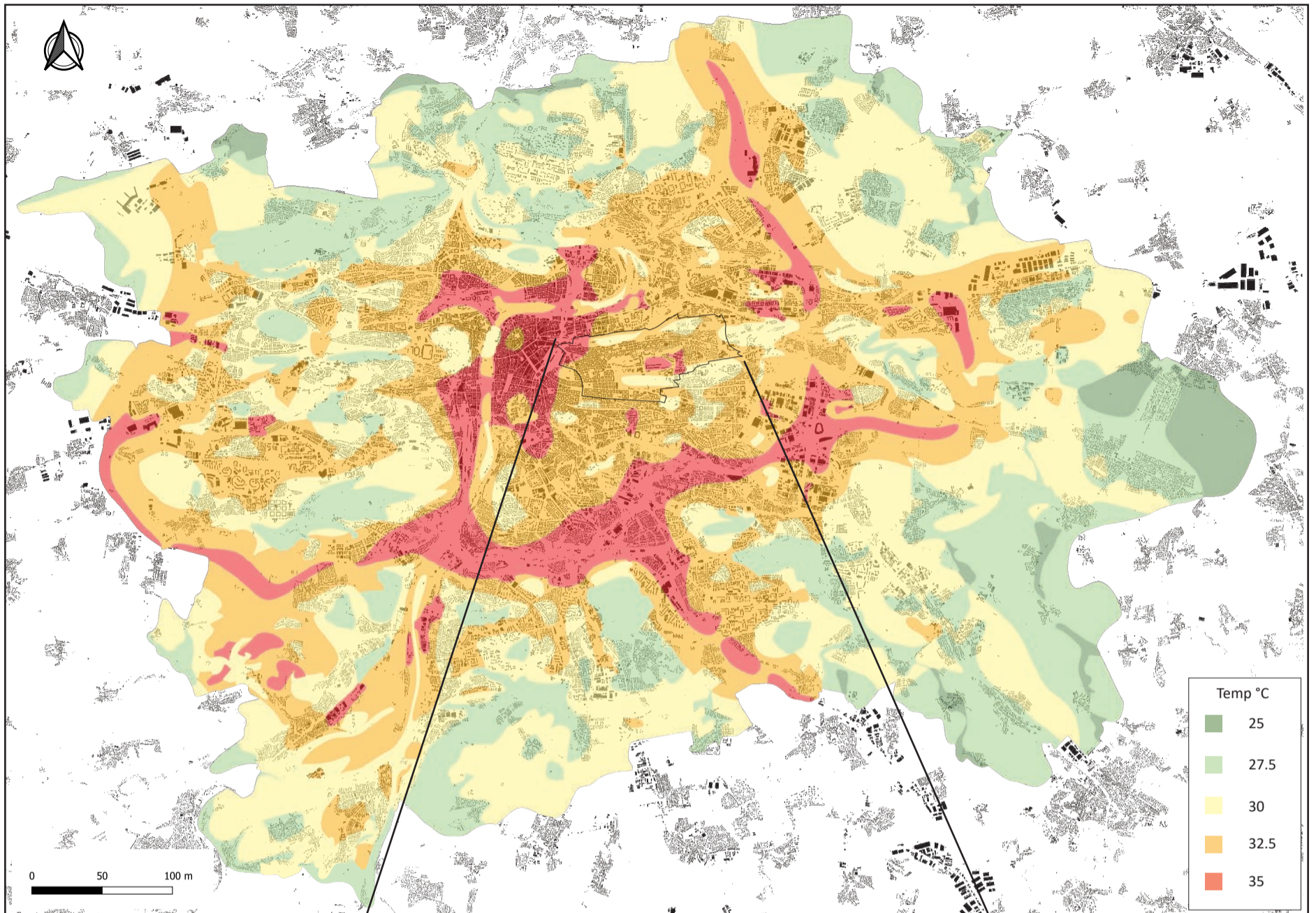
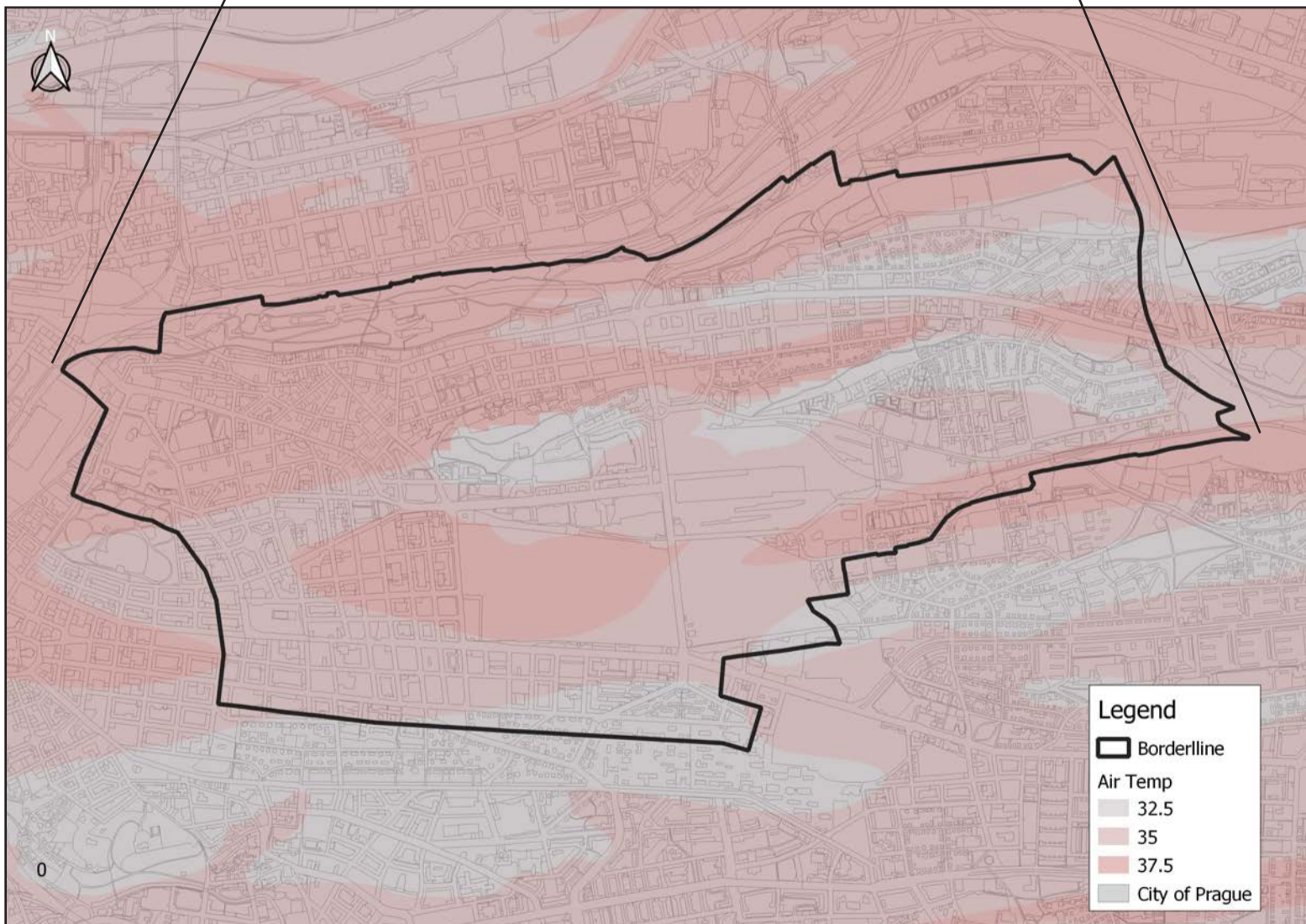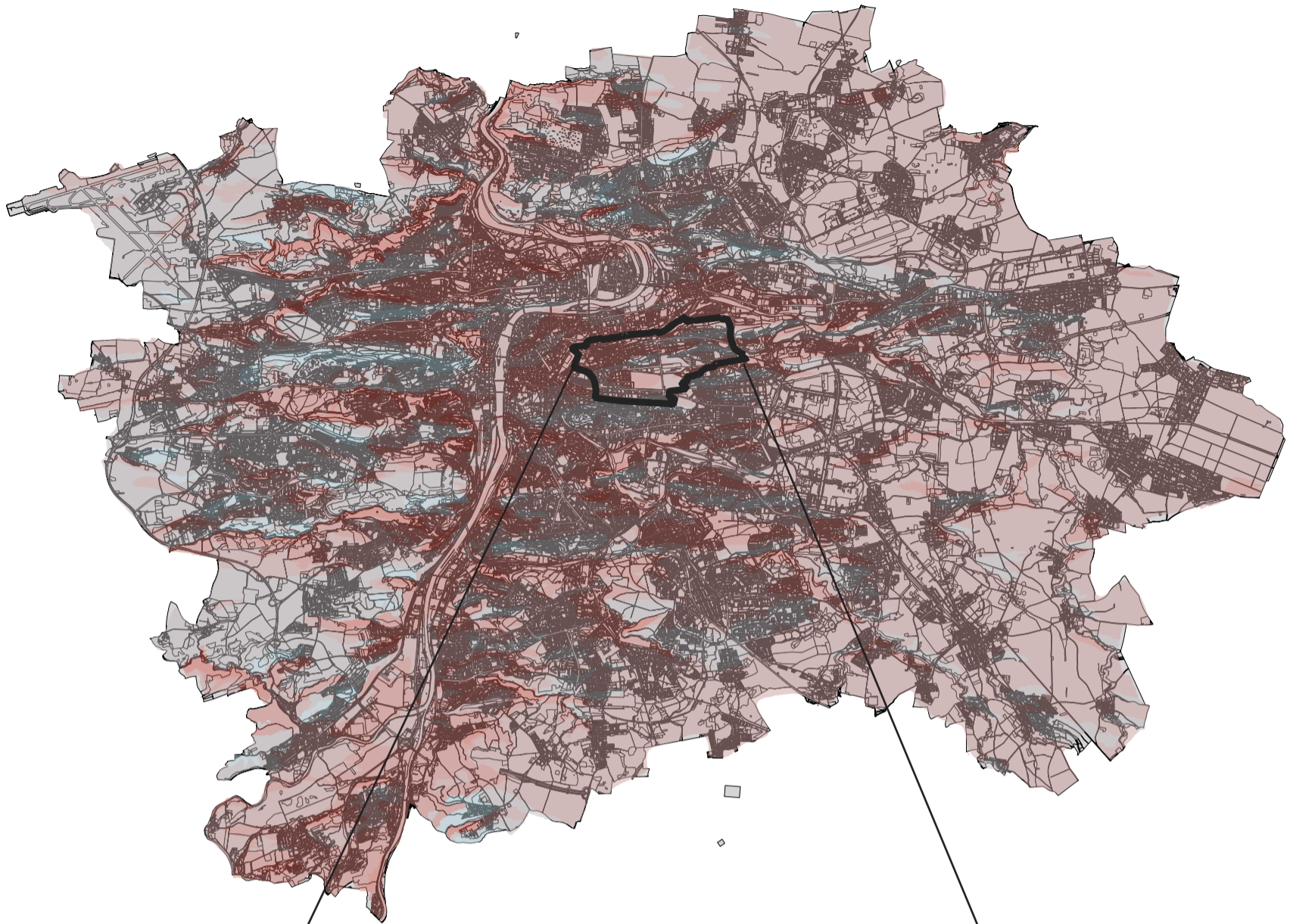Figure 5.1 : Surface Temperature above 30 °C in Prague
and Prague 3 (Author)

Figure 5.2 : Air Temperature above 30 °C in Prague and
Prague 3 (Author)

When comparing Figure No 5.1 and No 5.2, we can observe a different spatial representation of the warmest areas. This is because we are comparing the temperature limits of air and surface temperatures. Each surface has a different albedo and is differently susceptible to heat absorption. The distribution of air temperature, on the other hand, is more related to the topography of the city.

Similar to the surface temperature results, the most frequently represented surface use class for air temperature is continuous urban development (with stop density > 80%). In both cases of stressed surfaces, both by land and air temperatures, green urban areas, pastures and arable land appear in the list. Although the temperatures on these types of surfaces reached limit values (30 °C), thanks to their function and representation of greenery, they can dissipate heat much more efficiently. This is mainly due to evapotranspiration and its albedo. On green areas, where there is a demonstrably larger proportion of greenery, these values only lasted for less than 8 hours. On the contrary, continuous urban development can maintain accumulated heat for several hours. This idea is supported by Figure 4.4 together with table No. 5.1.3 and No. 5.1.4. shows for how long (number of hours) the temperature of 30 °C was exceeded in the area of interest.

Land Use classes	Number of surfaces
Wetlands	2
Complex and mixed cultivation patterns	4
Isolated structures	5
Mining and landfills	8
Discontinuous urban development with very low density (with building density <10%)	11
Construction site	17
Permanent crops (vineyards, fruit trees, olive groves)	18
Rapid transit roads and related lands	21
Discontinuous low-density urban development (with built-up density: 10% - 30%)	21
Herbaceous vegetation associations	31
Land without current use	57
Discontinuous urban development of medium density (with built-up density: 30% - 50%)	57
Pasture	81
Water surfaces	86
Forests	90
Sports and leisure facilities	114
Railway and related land	128
Fertile ground	319
Green urban areas	339
Industrial, commercial and private units	675
Other roads and related land	828
Discontinuous dense urban development (with built-up density: 50% - 80)	896
Continuous urban development (with built-up density > 80%)	926

Graph 5.1.3 : The number of areas (one area is approx. 100 x 100 m) in the territory of Prague, where a temperature of 30 °C was reached for 1 hour (author).

The fact that greenery can actively break down accumulated heat faster than high albedo surfaces is demonstrated by the following tabular representation. Table no. 5.1.4 shows that areas with low albedo: Contiguous urban development (with building density > 80%); Discontinuous dense urban development (with a building density of 50% - 80%); Other roads and related land; industrial, commercial and private units are abundantly represented here. However, there are also areas with a high albedo, greater humidity, and, in addition, with evapotranspiration and cooling effects - green and watery urban areas.

From table no 5.1.4, which shows areas where the temperature exceeded 30 °C for 8 hours, it is clear that these are only areas with a low albedo and with almost zero heat dissipation capabilities. Green and water areas are no longer present here (perhaps in negligible quantities), as they have managed to cope with the accumulated heat with the help of evapotranspiration, or by removing heat with the help of windy conditions.

Land use class	Number of surfaces
Contiguous urban development (with built-up density > 80%)	17
Other roads and related land	6
Industrial, commercial and private units	4
Discontinuous dense urban development (with a built-up density of 50% - 80%)	1

Graph 5.1.4 : The number of pixels (one area is approx. 100 x 100 m) in the territory of Prague, where a temperature of 30 °C was reached for 8 hours (author).

The main output of the work, graph No. 5.1.5, shows the distribution of air temperature values for individual UA2018 types using a box diagram at times when the 30 °C limit was exceeded, i.e., between 10:00 a.m. and 7:00 p.m. It shows that the highest air temperatures were reached on the UA2018 classes continuous urban development (with building density > 80%), discontinuous dense urban development (with building density 50% - 80%) and on the class other roads and related land. Temperatures reached up to 34°C on these three most susceptible UA2018 classes. The period between 10:00 and 19:00, when temperatures in the area of interest were above 30 °C, was closely monitored. Specifically, for the continuous urban development class (with a building density > 80%), the average air temperature during the observed period was 29.2 °C (with a maximum and minimum temperature of 34.3 and 24 °C). In discontinuous dense urban development (with a building density of 50% - 80%), the average

temperature was 29.04 °C (with a maximum and minimum temperature of 34.14 and 23 °C) mainly in the late afternoon (18:00 - 19:00)). The last type of LC monitored is the class of other roads and related land. In the territories of this class, average temperatures reached the limit of 29.64 °C. The maximum values reached air temperature values of 34.86 °C. The minimum values ranged around 22 °C (in the afternoon at 19:00).

On the contrary, the lowest monitored values in the area of interest were achieved by areas with the use class: Arable land, forests, permanent crops, and the class of other roads and related land. On these surface types, the average temperature ranged from 28°C to 29.64°C. The average temperature in the areas of class UA2018 - arable land was 28.21 °C. The maximum measured temperature was 31.26 °C. The minimum value, measured in the afternoon at 19:00, was around 22 °C. The UA2018 forest class had average temperature values equal to 28.23 °C. The maximum values (reached between 12:00 and 14:00) exceeded the 31 °C threshold by a hundredths. The minimums for this class were also measured in the afternoon (19:00) and were approximately equal to 22 °C. Average temperatures in the areas of the permanent culture class reached 28.25 °C. The maximum value was 31.6 °C, and the minimum was reached by this class in the morning (10:00) at a value of 21.13 °C.

Other temperature data were selected and summarized from an extensive tabular view exported from the ArcMap application, the table had over 35,000 rows and so it was impossible to attach it to the work in the appendices. The map output to the mentioned table can be found in Appendix No. 25. The class of other roads and related plots appears in both selections (On the list of areas that fared the worst and on those that fared better), due to the ability of the surface to break down the accumulated heat. For green areas, this principle is explained in chapter no. 3.6.1 and 3.6.2. Artificial materials (asphalt, concrete) have a reduced ability to evaporate, and because of their low albedo values, they are the materials with the greatest heat absorption.

From the analysis, it is clearly evident that areas with a greater proportion of greenery had clearly lower surface and air temperatures. It is also obvious that green and water areas may reach critical values, but only for a short period of the hottest day. For non-natural types of surfaces, the analysis showed the exact opposite. The temperatures remained in the most susceptible places for up to 8 hours before their values began to demonstrably decrease. At the same time, natural types of surfaces showed signs of cooling much earlier.

The concentration of green areas in the areas of continuous urban development (with built-up density > 80%), discontinuous dense urban development (with built-up density 50% - 80%) and on avenues other roads and related land should be increased so that these areas show the same in the future results as green urban areas, for housing types represented by UA2018 classes: Medium-density non-contiguous urban development (with building density: 30%-50%), low-density non-contiguous urban development (with building density: 10%-30%), very dense urban development with
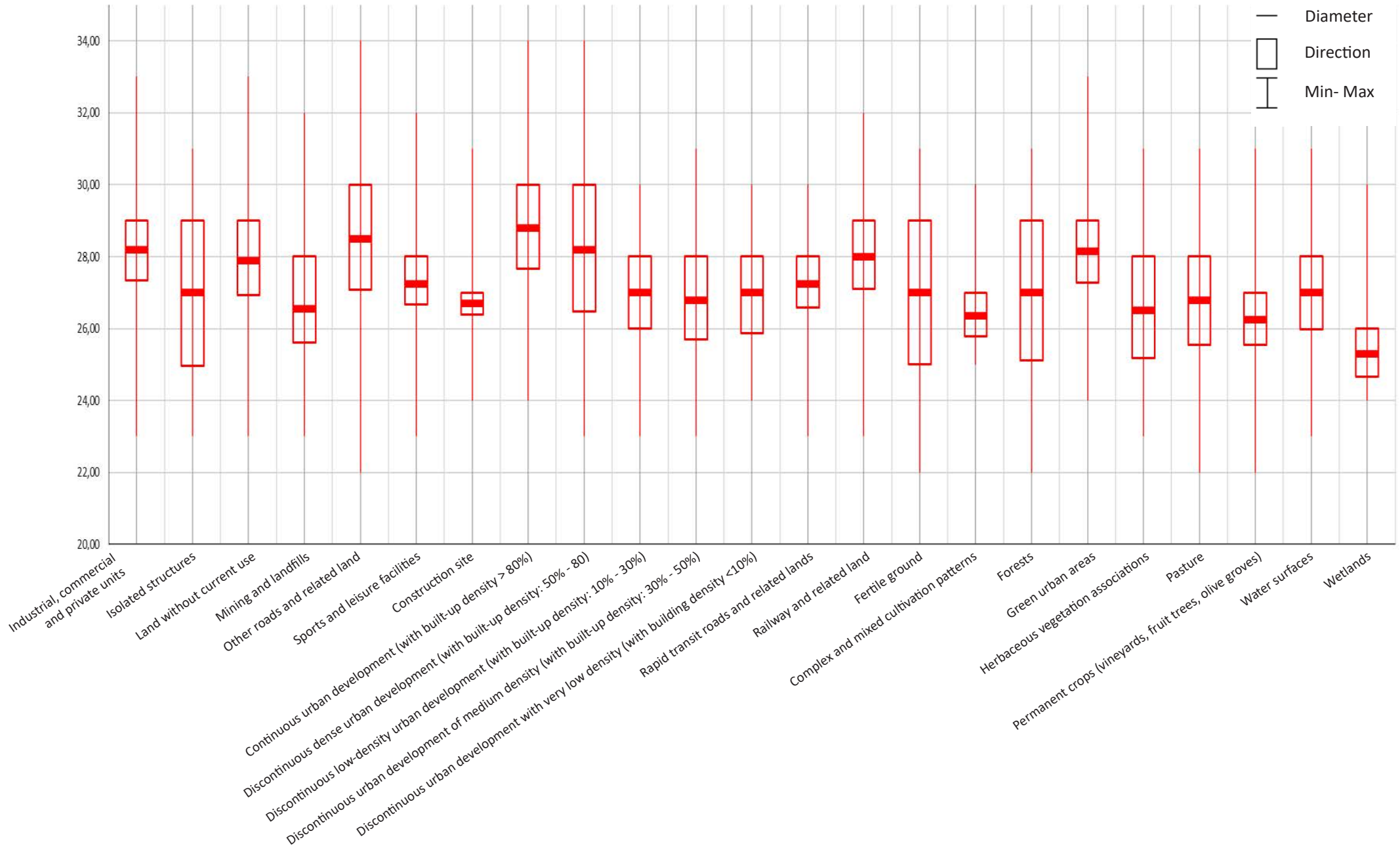
Graph 5.1.5: Characteristic air temperature values for individual classes of land use. Air temperature values were taken by the MUKLIMO_3 model between June and August 2022 (author).

low density (with building density <10%), it can be assumed that there is a higher proportion of greenery and thus a higher degree of thermal comfort. Urbanized areas, where the air temperature exceeds 34 °C in places or their close neighboring areas, are densely built up. It can, therefore, be said with certainty that the comfort of the residents here is greatly inconvenienced by the high flows of sensible heat. In these areas, it is necessary to fundamentally increase the representation of greenery or to change the materials used for the construction or renovation of infrastructure.

This can be achieved by implementing green roofs or green walls or using materials with a lower albedo. Warming buildings and thus reducing their energy dependence would result in a reduction in waste heat production and thereby reduce one of the essential input factors that make cities warmer than in other areas.

6. Discussion

The purpose of this work was to find a connection between the spatial distribution of air temperature during the passage of a heat wave in Prague in relation to various land use types. Air temperature data from the MUKLIMO_3 model was used to process this analysis. The results of the analysis were compared with surface temperature data from the Landsat 8 satellite and observed data from meteorological stations in Prague–Libuš and Ruzyn.

The results of this work confirm findings from previous studies. The amount of greenery in the city has a direct effect on the spatial distribution of air temperature and surface temperature. Areas with a higher proportion of greenery did not reach such high temperatures as areas with a lower proportion of greenery or none. From the results of the purposeful analysis, it was observed that the UA2018 classes, in which there is a greater proportion of greenery are up to 3 °C cooler than areas with dense urban development and areas of the infrastructure network.

Urban greenery plays an irreplaceable role in the urban climate. This is mentioned by Torbjörn and Bjorn, 2001, Konsova , 2019 and Savio et al., 2006.

Torbjörn and Bjorn, 2001 demonstrated in their research that by increasing the proportion of greenery, the city cools down more efficiently and quickly and does not overheat as it would without the presence of greenery. This fact was also confirmed by the analysis in this work. According to Coutts et al. (2016), the importance of the design and character of urban greenery is important with regard to their cooling potential. However, certain planning principles must be followed, otherwise increasing this share may even be counterproductive. By increasing the proportion of greenery by 30%, the air temperature increased in Torbjörn and Bjorn's study, which is an undesirable effect. In the work, it was proven that there are demonstrably higher temperatures on areas with a greater proportion of greenery. However, the shares of greenery in individual classes of land use are not represented in the results of the work, as the metadata of the input data did not contain such data.

Konsova's research followed the overall development of temperatures in Prague. This work focused only on surfaces where the temperature exceeded 30 °C because further increase of the temperature will change to a phenomenon as known as tropical day . This causes results from the same input data to have different results. However, the conclusion and starting points of both researches remain the same. As a background layer, Konsova used the Local Climate Zones landscape cover layer (Demuzere et al. 2022), which divides the urban development into several classes according to the density of the development, the height distribution of the development and the type of land use, similar to UA2018 (Copernicus, 2023). UA2018 does not separate the height variability of the building, which is a significant factor in some analyses. This work came to the values that the air temperature on urban green areas is lower than on other built-up areas. In the observed time range (10:00–19:00), when the temperature exceeded 30 °C in the investigated area, the temperature difference was on average 1.5 °C. Temperatures in the urban built-up area ranged between 29.04-29.64 °C. In green urban areas, the average air temperature ranged from 28.21–28.25 °C.

Air Temperature in Prague, June-August 2022
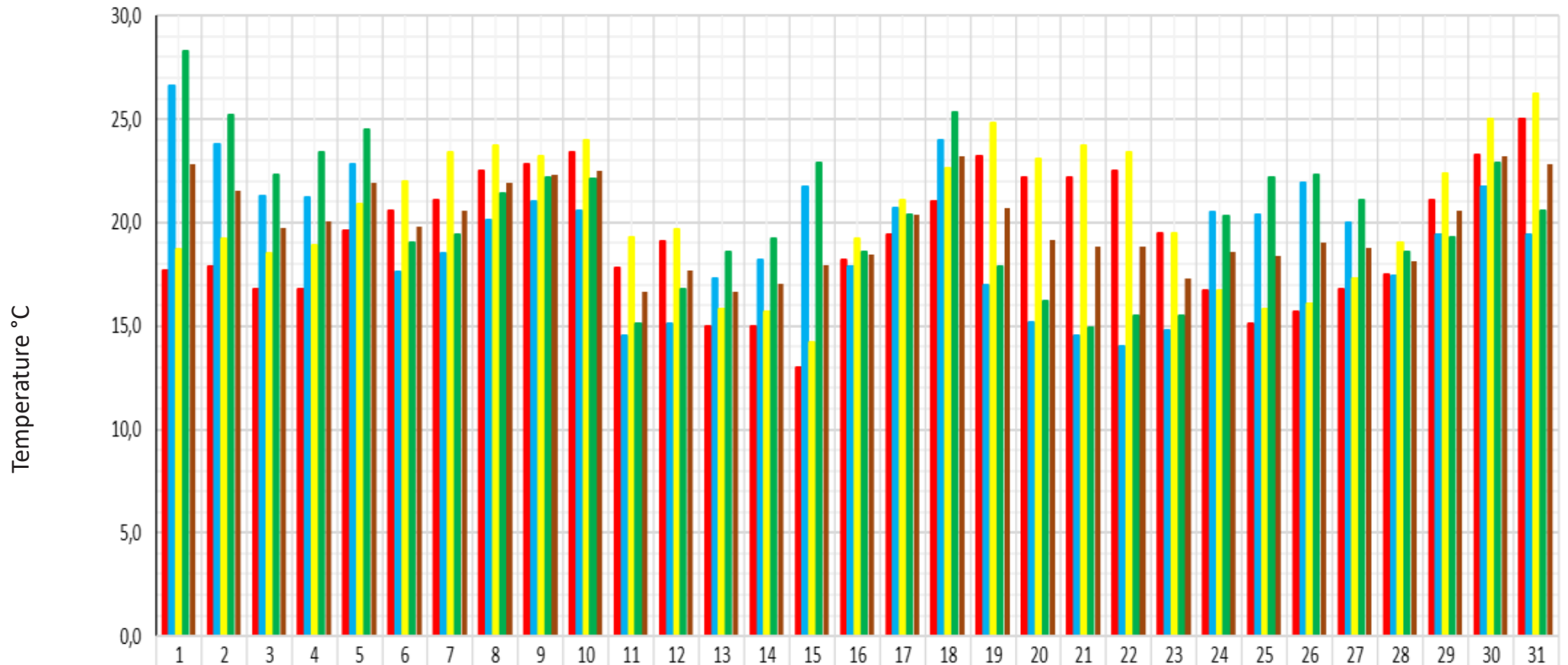
Time Course (Day)	1	2	3	4	5	6	7	8	9	10	11	12	13	14	15	16	17	18	19	20	21	22	23	24	25	26	27	28	29	30	31
Prague- Ruzyne (Jun)	17,7	17,9	16,8	16,8	19,6	20,6	21,1	22,5	22,8	23,4	17,8	19,1	15,0	15,0	13,0	18,2	19,4	21,0	23,2	22,2	22,2	22,5	19,5	16,7	15,1	15,7	16,8	17,5	21,1	23,3	25,0
Prague- Ruzyne (Aug)	26,6	23,8	21,3	21,2	22,8	17,6	18,5	20,1	21,0	20,6	14,5	15,1	17,3	18,2	21,7	17,9	20,7	24,0	17,0	15,2	14,5	14,0	14,8	20,5	20,4	21,9	20,0	17,4	19,4	21,7	19,4
Prague- Libus (Jun)	18,7	19,2	18,5	18,9	20,9	22,0	23,4	23,7	23,2	24,0	19,3	19,7	15,8	15,7	14,2	19,2	21,1	22,6	24,8	23,1	23,7	23,4	19,5	16,7	15,8	16,1	17,3	19,0	22,4	25,0	26,2
Prague- Libus (Aug)	28,3	25,2	22,3	23,4	24,5	19,0	19,4	21,4	22,2	22,1	15,1	16,8	18,6	19,2	22,9	18,6	20,4	25,3	17,9	16,2	14,9	15,5	15,5	20,3	22,2	22,3	21,1	18,6	19,3	22,9	20,6
Average Values	22,8	21,5	19,7	20,1	22,0	19,8	20,6	21,9	22,3	22,5	16,7	17,7	16,7	17,0	18,0	18,5	20,4	23,2	20,7	19,2	18,8	18,9	17,3	18,6	18,4	19,0	18,8	18,1	20,6	23,2	22,8

Prague- Ruzyne (Jun) Prague- Ruzyne (Aug) Prague- Libus (Jun) Prague- Libus (Aug) Average Values

Graph 6.1.1: The average air temperature in the capital city of Prague at two measuring stations (Ruzyne-Libus)

The average temperatures are compared with the values of two measuring stations of Prague in chart no. 5.1.5 between (Jun-Aug, 2022). For Prague - Ruzyně the temperature was 23.3 °C and for Prague - Libuš it was 25 °C.

In table no. 6.1.2, we can observe the subtraction of the average temperature values at the measuring stations from the extracted temperatures value. Model air temperatures were higher by more than +4 °C (for the "Other roads and associated land" class, the temperature even exceeded the temperature average by +6.34 °C). High air temperature can, according to Dobrovolný et al. (2012) also influence the surfaces on which it moves. Due to the high air temperature, the surfaces heat up more than under normal conditions, and thus take longer to cool down. This increases the time that urban areas are exposed to thermal stress, creating the *Urban Heat Island* effect. The difference between these temperatures and the values obtained in the work is obvious from spatial observation. Like Libuš, Ruzyně is a peripheral area of the capital. Ruzyň is located at an altitude of 330 m above sea level and Libuš is at an altitude of 300 m above sea level. This is only a spot monitoring of the air temperature, in the analysis of the work the entire territory of Prague is examined, therefore the temperature difference can be considerable.

Land use class	Average temperature (°C)	Comparison Prague - Ruzyně (+23.3°C)	Comparison Prague - Libuš (+25 °C)
Contiguous urban development (with built-up density > 80%)	+29.22	+5.92	+4.22
Discontinuous dense urban development (with a built-up density of 50% - 80%)	+29.04	+5.74	+4.04
Other roads and related land	+29.64	+6.34	+4.64
Fertile ground	+28.21	+4.91	+3.21
Forests	+28.23	+4.93	+3.23
Permanent crops	+28.25	+4.95	+3.25

Graph 6.1.2: Comparison of average air temperatures over selected land use classes according to the MUKLIMO_3 model with average daily air temperature values measured at ČHMÚ stations on Sep 2022 (author)

At the same time, different values were measured at two measuring stations. This can also be caused by several other factors (type of land use, weather conditions, height of buildings in the vicinity of the ratio of greenery and buildings in a given

area). As described later in the text, altitude also plays a role in the observation of temperature phenomena.

The average temperature decreases with increasing altitude by 0.6 °C for every 100 meters of altitude (ČHMÚ, 2012). Which explains the temperature difference between the measuring stations. However, from the analysis carried out, the temperature mainly depends on the type of land use. From Figure 5.3, we can see that the surface temperature exceeded the 30 °C mark, mainly in the valley near the Vltava river.

The analysis of the temperature dependence on the altitude is rather marginal and to supplement and clarify some of the measured values. It is evident that altitude plays a role in the temperature analysis of susceptible areas, but the key factor here is land use class. It is very difficult to determine the unequivocal influence of altitude in the area of interest. Due to the low range of altitudes, which range from 175 to 388 meters above sea level.

Nevertheless, some conclusions can be drawn from the analysis of the shaded relief and surface temperature data. It is evident that capital city of Prague is the most susceptible area, which locates in an altitude from 200 to 290 m above sea level. (see Figure 6.1). Most of the continuous urban development (with a population density > 80%) and other roads and related land, industrial commercial and private buildings are located in these heights. Greenery here is represented by parks or haphazard rows of trees, which cannot effectively cool such vast areas. In the higher areas of Prague, there is a rugged terrain on which, for the time being, green areas prevail over built-up ones. In this respect, altitude did not play a major role. Due to its height variability, Prague forms a relatively small monitored scale. More accurate conclusions would be brought by the research of a city with greater variability in altitude. From the observation made above, it can be seen that the occurrence of minimum and maximum afternoon temperatures is not only dependent on the land use class, but it is dependent on many other factors. The type of land cover can have a similar influence as the category of land use type. Here, green areas are able to break down the accumulated heat more efficiently and thereby reduce the intensity of the surface urban island. Another can be the distribution of buildings on a given area, the density of buildings or the degree of obscuring the horizon by obstacles or altitude (Dobrovolný et al. 2012). From the surface temperature in figure no. 5.3, however, it can be seen that the surface temperature was distributed more randomly in the territory of Prague, which indicates a greater influence of the land use class.

Figure 6.1: Frequency of temperature stressed surfaces at individual altitudes
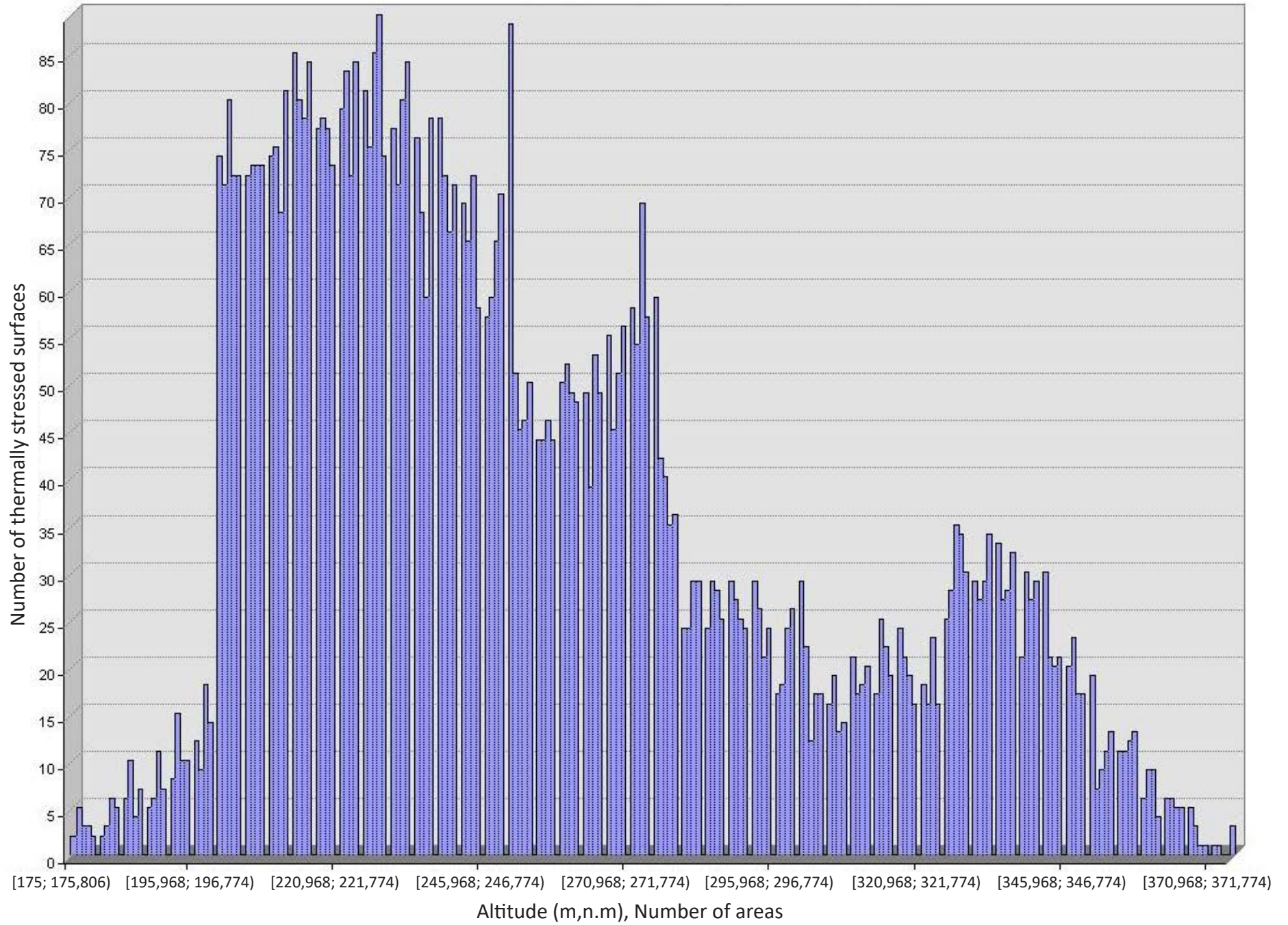
7. Conclusion

The main goal of the work was the processing of model temperature data within the MUKLIMO_3 heat wave and data obtained from Landsat 8 scanning in between Jun-Aug 2022 in the investigated area, which was the capital city of Prague, Prague 3 and further evaluation of the dependence of the temperature data on the functional use of the territory Urban Atlas 2018. For the purpose of visualization of the results, map outputs were developed, which complemented the tabular display of the data resulting from the analysis.

The first part of the thesis dealt with the theoretical research of urban climate issues, the formation of the urban heat island and the factors influencing its formation. Furthermore, climatic changes were briefly described, the terms surface temperature and air temperature, heat waves, which were necessary for the further context of the work, were explained. The last chapters in the research were chapters related to the types of land use and land cover.

The main part of the work dealt with the processing and analysis of temperature data from the MUKLIMO_3 model and data from the Landsat 8 satellite, depending on land use classes. It is evident from the results of the work that areas with a larger share of greenery are less thermally stressed than areas where the representation of greenery is smaller. According to the analysis of air temperatures, the worst classes of land use were densely built-up urban areas (with a built-up density above 50%), roads and industrial, commercial and private units. Areas with a higher percentage of greenery, such as arable land, forests, and permanent crops, fared slightly better. In conclusion, it can be argued that the center of Prague achieved worse results in the analysis than the peripheral areas. This is determined by the structure of the building and the lack of green areas. Then the dependence of temperature data on altitude was briefly described, which in Prague is rather a complementary factor in terms of the low variability of this altitude. However, areas located at a lower altitude showed a greater susceptibility to the accumulation of air temperatures. As for the surface temperature, the altitude was rather negligible, as the temperature-stressed places were randomly distributed. The determining factor here was the land use class.

In conclusion, it can be said that it would be good to increase the share of greenery in places under temperature stress and, if possible, replace dark materials with materials with a higher albedo in the infrastructure.

The benefit of this work is mainly the processing of surface temperature data, air temperature and the identification of areas that have a higher tendency to overheat. At the same time, these areas have a lower ability to dissipate heat, as there is insufficient representation of greenery. This is important for the implementation of adaptation measures in future years.

8. References

1. A review on the generation, determination and mitigation of Urban Heat Island—ScienceDirect. (n.d.). Retrieved March 11, 2024, from https://www.sciencedirect.com/science/article/abs/pii/S1001074208600194

2. Abd Elraouf, R., Elmokadem, A., Megahed, N., Eleinen, O., & Eltarabily, S. (2022). The impact of urban geometry on outdoor thermal comfort in a hot-humid climate. Building and Environment, 225, 109632. https://doi.org/10.1016/j.buildenv.2022.109632

3. Akbari, H., Pomerantz, M., & Taha, H. (2001a). Cool surfaces and shade trees to reduce energy use and improve air quality in urban areas. Solar Energy, 70(3), 295–310. https://doi.org/10.1016/S0038-092X(00)00089-X

4. Akbari, H., Pomerantz, M., & Taha, H. (2001b). Cool Surfaces and Shade Trees to Reduce Energy Use and Improve Air Quality in Urban Areas. Solar Energy, 70, 295–310. https://doi.org/10.1016/S0038-092X(00)00089-X

5. Asaeda, T., Ca, V. T., & Wake, A. (1996). Heat storage of pavement and its effect on the lower atmosphere. Atmospheric Environment, 30(3), 413–427. https://doi.org/10.1016/1352-2310(94)00140-5

6. Asimakopoulos, D. A., Santamouris, M., Farrou, I., Laskari, M., Saliari, M., Zanis, G., Giannakidis, G., Tigas, K., Kapsomenakis, J., Douvis, C., Zerefos, S. C., Antonakaki, T., & Giannakopoulos, C. (2012). Modelling the energy demand projection of the building sector in Greece in the 21st century. Energy and Buildings, 49, 488–498. https://doi.org/10.1016/j.enbuild.2012.02.043

7. Asimakopoulos, D. N. (2001). Energy and Climate in the Urban Built Environment. Earthscan.

8. Bocquier, P. (2005). World Urbanization Prospects: An alternative to the UN model of projection compatible with the mobility transition theory. Demographic Research, 12, 197–236.

9. Buettner, K. J. K., & Kern, C. D. (1965). The determination of infrared emissivities of terrestrial surfaces. Journal of Geophysical Research (1896-1977), 70(6), 1329–1337. https://doi.org/10.1029/JZ070i006p01329

10. Changnon, S. A., Kunkel, K. E., & Reinke, B. C. (1996). Impacts and Responses to the 1995 Heat Wave: A Call to Action. Bulletin of the American Meteorological Society, 77(7), 1497–1506. https://doi.org/10.1175/1520-0477(1996)077<1497:IARTTH>2.0.CO;2

11. De Rose, A., & Di Cesare, M. (2003). Genere e scioglimento della prima unione (pp. 339–365).

12. Del Savio, A., Andrade, S. A. L., Martha, L., Vellasco, P., & Lima, L. (2006). Semi-rigid portal frame finite element modelling including the axial versus bending moment interaction in the structural joints. Proceedings of the International Colloquium on Stability and Ductility of Steel Structures, SDSS 2006, 389–396.

13. Development and testing of thermochromic coatings for buildings and urban structures | Request PDF. (n.d.). Retrieved March 11, 2024, from https://www.researchgate.net/publication/229398244_Development_and_testing_of_

thermochromic_coatings_for_buildings_and_urban_structures

14. Doulos, L., Santamouris, M., & Livada, I. (2004). Passive Cooling of Outdoor Urban Spaces. The Role of Materials. Solar Energy, 77, 231–249. https://doi.org/10.1016/j.solener.2004.04.005

15. Easterling, D. R., Evans, J. L., Groisman, P. Y., Karl, T. R., Kunkel, K. E., & Ambenje, P. (2000). Observed Variability and Trends in Extreme Climate Events: A Brief Review. Bulletin of the American Meteorological Society, 81(3), 417–426. https://doi.org/10.1175/1520-0477(2000)081<0417:OVATIE>2.3.CO;2

16. Figure 2.1: Factors of Urban Heat Island (UHI) (Rizwan et al, 2008). (n.d.). ResearchGate. Retrieved March 11, 2024, from https://www.researchgate.net/figure/Factors-of-Urban-Heat-Island-UHI-Rizwan-et-al-2008_fig4_306932682

17. Fontaine, B., Roucou, P., Gaetani, M., & Marteau, R. (2011). Recent changes in precipitation, ITCZ convection and northern tropical circulation over North Africa (1979–2007). International Journal of Climatology, 31(5), 633–648. https://doi.org/10.1002/joc.2108

18. Founda, D. (2011). Evolution of the air temperature in Athens and evidence of climatic change: A review. Advances in Building Energy Research, 5(1), 7–41. https://doi.org/10.1080/17512549.2011.582338

19. Gao, X., Shi, Y., Zhang, D., & Giorgi, F. (2012). Climate change in China in the 21st century as simulated by a high resolution regional climate model. Chinese Science Bulletin, 57(10), 1188–1195. https://doi.org/10.1007/s11434-011-4935-8

20. Gavin, D. G., Hallett, D. J., Hu, F. S., Lertzman, K. P., Prichard, S. J., Brown, K. J., Lynch, J. A., Bartlein, P., & Peterson, D. L. (2007). Forest fire and climate change in western North America: Insights from sediment charcoal records. Frontiers in Ecology and the Environment, 5(9), 499–506. https://doi.org/10.1890/060161

21. Golden, J., & Kaloush, K. (2006). Mesoscale and microscale evaluation of surface pavement impacts on the urban heat island effects. International Journal of Pavement Engineering - INT J PAVEMENT ENG, 7, 37–52. https://doi.org/10.1080/10298430500505325

22. Gui, N. M. M., Lee, K. T., & Bhatia, S. (2008). Feasibility of edible oil vs. Non-edible oil vs. Waste edible oil as biodiesel feedstock. Energy, 33, 1646–1653. https://doi.org/10.1016/j.energy.2008.06.002

23. Hansen, M. H., Li, H., & Svarverud, R. (2018). Ecological civilization: Interpreting the Chinese past, projecting the global future. Global Environmental Change, 53, 195–203. https://doi.org/10.1016/j.gloenvcha.2018.09.014

24. Haselbach, L. (2009). Potential for Carbon Dioxide Absorption in Concrete. Journal of Environmental Engineering-Asce - J ENVIRON ENG-ASCE, 135. https://doi.org/10.1061/(ASCE)EE.1943-7870.0000004

25. Hassid, S., Santamouris, M., Papanikolaou, N., Linardi, A., Klitsikas, N., Georgakis, C., & Assimakopoulos, D. N. (2000). The effect of the Athens heat island on air conditioning load. Energy and Buildings, 32(2), 131–141. https://doi.org/10.1016/S0378-7788(99)00045-6

26. Hermanson, L., & Sutton, R. (2010). Case studies in interannual to decadal climate predictability. Clim. Dyn., 35, 1169–1189. https://doi.org/10.1007/s00382-009-

0672-y

27. Jacobson, M. Z., & Ten Hoeve, J. E. (2012). Effects of Urban Surfaces and White Roofs on Global and Regional Climate. Journal of Climate, 25(3), 1028–1044. https://doi.org/10.1175/JCLI-D-11-00032.1

28. James, J. D., Spittle, J. A., Brown, S. G. R., & Evans, R. W. (2001). A review of measurement techniques for the thermal expansion coefficient of metals and alloys at elevated temperatures. Measurement Science and Technology, 12(3), R1. https://doi.org/10.1088/0957-0233/12/3/201

29. Jiji, L. (2009). Heat convection: Second edition. In Heat Convection: Second Edition (p. 543). https://doi.org/10.1007/978-3-642-02971-4

30. Kolokotsa, D., Santamouris, M., & Zerefos, S. C. (2013). Green and cool roofs' urban heat island mitigation potential in European climates for office buildings under free floating conditions. Solar Energy, 95, 118–130. https://doi.org/10.1016/j.solener.2013.06.001

31. Kolokotsa, D., Tsoutsos, T., & Papantoniou, S. (2012). Energy Conservation Techniques for Hospital Buildings. Advances in Building Energy Research, 1–14. https://doi.org/10.1080/17512549.2012.672007

32. Konopacki, S., & Akbari, H. (2002). Energy savings for heat-island reduction strategies in Chicago and Houston (including updates for Baton Rouge, Sacramento, and Salt Lake City). https://escholarship.org/uc/item/2rv7n2gn

33. Li, H., Huo, Y.-G., He, X., Yao, L., Zhang, H., Yiqiang, C., Xiao, H., Xie, W., Dejiu, Z., Wang, Y., Zhang, S., Tu, H., Cheng, Y., Guo, Y., Cao, X., Zhu, Y., Jiang, T., Guo, X., Qin, Y., & Sha, J. (2022). Li et al-2022-Nature. Nature, 2022, 1. https://doi.org/10.1038/s41586-022-05508-0

34. Livada, I., Santamouris, M., & Assimakopoulos, M. (2007). On the variability of summer air temperature during the last 28 years in Athens. Journal of Geophysical Research, 112. https://doi.org/10.1029/2006JD008140

35. Luber, G., & McGeehin, M. (2008). Climate change and extreme heat events. American Journal of Preventive Medicine, 35(5), 429–435. https://doi.org/10.1016/j.amepre.2008.08.021

36. Memon, R., Leung, D., & Chunho, L. (2008). A review on the generation, determination and mitigation of Urban Heat Island. Journal of Environmental Sciences (China), 20, 120–128. https://doi.org/10.1016/S1001-0742(08)60019-4

37. Menon, D., Schwab, K., Wright, D., & Maas, A. (2010). Position Statement: Definition of Traumatic Brain Injury. Archives of Physical Medicine and Rehabilitation, 91, 1637–1640. https://doi.org/10.1016/j.apmr.2010.05.017

38. Mihalakakou, G. (2002). On estimating soil surface temperature profiles. Energy and Buildings, 34(3), 251–259. https://doi.org/10.1016/S0378-7788(01)00089-5

39. Niachou, A., Papakonstantinou, K., Santamouris, M., Tsangrassoulis, A., & Mihalakakou, G. (2001). Analysis of the Green Roof Thermal Properties and Investigation of its Energy Performance. Energy and Buildings, 33, 719–729. https://doi.org/10.1016/S0378-7788(01)00062-7

40. Nonlinear temperature effects indicate severe damages to U.S. crop yields under climate change | PNAS. (n.d.). Retrieved March 11, 2024, from https://www.pnas.

org/doi/abs/10.1073/pnas.0906865106

41. Oleson, K. W., Bonan, G. B., Feddema, J., Vertenstein, M., & Grimmond, C. S. B. (2008). An Urban Parameterization for a Global Climate Model. Part I: Formulation and Evaluation for Two Cities. Journal of Applied Meteorology and Climatology, 47(4), 1038–1060. https://doi.org/10.1175/2007JAMC1597.1

42. Painting streets white. Great marketing, terrible idea. (2017, December 5). Home. https://www.gmccx.com/post/2017/12/04/painting-streets-white-great-marketing-terrible-idea

43. Pomerantz, M., Akbari, H., Chen, A., Taha, H., & Rosenfeld, A. H. (1997). Paving materials for heat island mitigation (LBL--38074, 291033; p. LBL--38074, 291033). https://doi.org/10.2172/291033

44. Prague City Hall | Prague for all. (n.d.). Retrieved March 11, 2024, from https://metropolevsech.eu/en/kontakty/urady-v-praze/magistrat-hl-m-prahy/

45. Qin, Y., & Hiller, J. E. (2011). Modeling the temperature and stress distributions in rigid pavements: Impact of Solar Radiation absorption and heat history development. KSCE Journal of Civil Engineering, 15(8), 1361–1371. https://doi.org/10.1007/s12205-011-1322-6

46. Rosenfeld, D., & Lensky, I. M. (1998). Satellite-Based Insights into Precipitation Formation Processes in Continental and Maritime Convective Clouds. Bulletin of the American Meteorological Society, 79(11), 2457–2476. https://doi.org/10.1175/1520-0477(1998)079<2457:SBIIPF>2.0.CO;2

47. Sailor, D. J. (1995). Simulated Urban Climate Response to Modifications in Surface Albedo and Vegetative Cover. Journal of Applied Meteorology and Climatology, 34(7), 1694–1704. https://doi.org/10.1175/1520-0450-34.7.1694

48. Sailor, D., Smith, M., & Hart, M. (2008). Climate change implications for wind power resources in the Northwest United States. Renewable Energy, 33, 2393–2406. https://doi.org/10.1016/j.renene.2008.01.007

49. Saka, C., & Oshika, T. (2014). Disclosure effects, carbon emissions and corporate value. Sustainability Accounting, Management and Policy Journal, 5(1), 22–45. https://doi.org/10.1108/SAMPJ-09-2012-0030

50. Santamouris, M., Paraponiaris, K., & Mihalakakou, G. (2007). Estimating the ecological footprint of the heat island effect over Athens, Greece. Climatic Change, 80(3), 265–276. https://doi.org/10.1007/s10584-006-9128-0

51. Şengel, Ü., & Koç, A. (2022). Bibliometric review of studies on sustainable tourism and climate change in 2019. Turismo y Sociedad, 31, 161–176. https://doi.org/10.18601/01207555.n31.09

52. Shin, H.-J., Jang, C. J., & Chung, I.-U. (2017). A linear projection for the timing of unprecedented climate in Korea. Asia-Pacific Journal of Atmospheric Sciences, 53(4), 411–419. https://doi.org/10.1007/s13143-017-0044-1

53. Simulation of surface urban heat islands under 'ideal' conditions at night part 2: Diagnosis of causation | Boundary-Layer Meteorology. (n.d.). Retrieved March 11, 2024, from https://link.springer.com/article/10.1007/BF00119211

54. Slope Homogeneity Test (Pesaran and Yamagata 2008). (n.d.). ResearchGate. Retrieved March 11, 2024, from https://www.researchgate.net/figure/Slope-

Homogeneity-Test-Pesaran-and-Yamagata-2008_tbl2_373360252

55. Stathopoulou, M., Synnefa, A., Cartalis, C., Santamouris, M., Karlessi, T., & Akbari, H. (2009). A surface heat island study of Athens using high-resolution satellite imagery and measurements of the optical and thermal properties of commonly used building and paving materials. International Journal of Sustainable Energy, 28(1–3), 59–76. https://doi.org/10.1080/14786450802452753

56. Stathopoulou, O. I., Assimakopoulos, V. D., Flocas, H., & Helmis, C. (2008). An experimental study of air quality inside large athletic halls. Building and Environment, 43, 834–848. https://doi.org/10.1016/j.buildenv.2007.01.026

57. Synnefa, A., Dandou, A., Santamouris, M., Tombrou, M., & Soulakellis, N. (2008). On the Use of Cool Materials as a Heat Island Mitigation Strategy. Journal of Applied Meteorology and Climatology - J APPL METEOROL CLIMATOL, 47, 2846–2856. https://doi.org/10.1175/2008JAMC1830.1

58. Synnefa, A., Santamouris, M., & Livada, I. (2006). A study of the thermal performance of reflective coatings for the urban environment. Solar Energy, 80(8), 968–981. https://doi.org/10.1016/j.solener.2005.08.005

59. Taha, R., Al-Harthy, A., Al-Shamsi, K., & Al-Zubeidi, M. (2002). Cement Stabilization of Reclaimed Asphalt Pavement Aggregate for Road Bases and Subbases. Journal of Materials in Civil Engineering, 14(3), 239–245. https://doi.org/10.1061/(ASCE)0899-1561(2002)14:3(239)

60. ÚAP Praha 2020. (n.d.). Retrieved March 11, 2024, from https://uap.iprpraha.cz/#/

61. White, C. R., Phillips, N. F., & Seymour, R. S. (2005). The scaling and temperature dependence of vertebrate metabolism. Biology Letters, 2(1), 125–127. https://doi.org/10.1098/rsbl.2005.0378

62. Xu, C., McDowell, N. G., Fisher, R. A., Wei, L., Sevanto, S., Christoffersen, B. O., Weng, E., & Middleton, R. S. (2019). Increasing impacts of extreme droughts on vegetation productivity under climate change. Nature Climate Change, 9(12), 948–953. https://doi.org/10.1038/s41558-019-0630-6

63. Xue, C., Shahbaz, M., Ahmed, Z., Ahmad, M., & Sinha, A. (2022). Clean energy consumption, economic growth, and environmental sustainability: What is the role of economic policy uncertainty? Renewable Energy, 184, 899–907. https://doi.org/10.1016/j.renene.2021.12.006